



Extent and retreat history of the Barra Fan Ice Stream offshore western Scotland and northern Ireland during the last glaciation

S. Louise Callard ^{a,*}, Colm Ó. Cofaigh ^a, Sara Benetti ^b, Richard C. Chiverrell ^c,
Katrien J.J. Van Landeghem ^d, Margot H. Saher ^d, Jenny A. Gales ^e, David Small ^a,
Chris D. Clark ^f, Stephen, J. Livingstone ^f, Derek Fabel ^g, Steven G. Moreton ^h

^a Department of Geography, Durham University, Durham, DH1 3LE, UK

^b School of Geography and Environmental Sciences, Ulster University, Coleraine, BT52 1SA, Ireland

^c Department of Geography, University of Liverpool, Liverpool, UK

^d School of Ocean Sciences, Bangor University, Menai Bridge, UK

^e University of Plymouth, School of Biological and Marine Sciences, Drake Circus, Plymouth, PL4 8AA, UK

^f Department of Geography, University of Sheffield, Sheffield, S10 2TN, UK

^g Scottish Universities Environmental Research Centre, University of Glasgow, East Kilbride, G75 0QF, UK

^h Natural Environment Research Council, Radiocarbon Facility, East Kilbride, Scotland, G75 0QF, UK

ARTICLE INFO

Article history:

Received 19 January 2018

Received in revised form

27 September 2018

Accepted 2 October 2018

Keywords:

British-Irish Ice Sheet

Glacimarine

Last glacial maximum

Radiocarbon dating

Ice-sheet retreat

Grounding-zone wedges

ABSTRACT

During the Last Glacial Maximum (LGM) the marine-terminating Barra Fan Ice Stream (BFIS), a major conduit of the British Irish Ice Sheet (BIIS), drained much of western Scotland and northwest Ireland with ice streaming onto the continental shelf of the Malin Sea. The extent and retreat history of this ice stream across the shelf, until now, is not well known. In particular, geochronological constraints on the history of this ice stream have thus far been restricted to deep-sea cores or terrestrial cosmogenic nuclide dating onshore, with ages across the shelf absent. To understand the possible external forcing factors acting on this marine terminating ice stream during retreat, improved geochronological constraint on its deglaciation is necessary. Here, we present new geophysical data, marine sediment cores and over forty radiocarbon dates to provide important constraints on maximum extent of the BFIS, as well as the timing and pattern of retreat back across the Malin Shelf. Dated moraines and grounding-zone wedges (GZW) seen in seafloor sub-bottom profiles provide evidence that the BFIS reached the Malin Shelf edge during the LGM and was at its maximum extent around 26.7 ka BP. The presence of two sets of GZWs suggests that the style of retreat was episodic. The new radiocarbon chronology shows that retreat from the shelf edge was underway by 25.9 ka BP, with the majority of the continental shelf ice free by 23.2 ka BP, and that glacimarine conditions were present in the Sea of Hebrides by 20.2 ka BP at the latest. Collectively, these results indicate that the majority of the Malin Shelf was free of grounded ice by ~21.5–20 ka BP, which is up to 4000 years earlier than previously reconstructed. We attribute this early deglaciation to high relative sea level caused by glacial isostatic depression when the BIIS reached its maximum extent promoting ice shelf and grounding line instability. Two deep troughs, forming reverse bed slopes, aided the continued retreat of the BFIS. This suggests that local ice loading and bed morphology can be significant controls on the destabilisation of a marine-terminating ice stream and can override the influence of ocean and atmospheric temperatures.

© 2018 The Authors. Published by Elsevier Ltd. This is an open access article under the CC BY license (<http://creativecommons.org/licenses/by/4.0/>).

1. Introduction

During the Last Glacial Maximum (LGM) defined here as ca.

26.5–19 ka (P.U. Clark et al., 2009) the British-Irish Ice Sheet (BIIS) extended to the continental shelf break offshore of western Ireland and Scotland (Bradwell et al., 2008; Clark et al., 2012; Ó Cofaigh et al., 2012, 2016; Peters et al., 2015, 2016). Despite the global eustatic sea level being 134 m lower than present (Lambeck et al., 2014), up to two thirds of the BIIS was marine influenced and was drained by ice streams (Clark et al., 2012). It is therefore likely

* Corresponding author.

E-mail address: louise.callard@durham.ac.uk (S.L. Callard).

that the BIIS was sensitive to both oceanic and atmospheric changes, both major forcing factors in deglaciation (Clark et al., 2012). The BIIS is therefore a good analogue for the West Antarctic Ice Sheet (WAIS) and Greenland Ice Sheet, which are currently undergoing rapid thinning and retreat of marine-based sectors (Joughin et al., 2014; Mouginot et al., 2015). Predicting the impact of these changes, particularly with respect to sea level, requires modelling informed by empirical data on the processes, rates and controls of palaeo-marine based ice stream retreat (Hindmarsh, 2018). Reconstructing the deglaciation of the BIIS will therefore provide valuable empirical data to test and inform ice sheet models. Although recent research offshore Britain and Ireland, using marine geophysical data, has significantly enhanced our understanding of the glacial geomorphology of the shelf (e.g. Benetti et al., 2010; Dunlop et al., 2010; Ó Cofaigh et al., 2012), the extent and dynamic retreat of most of the marine-based sectors of the BIIS are still not well constrained chronologically.

During the LGM, the Barra Fan Ice Stream (BFIS; Dove et al., 2015) drained at least 5–10% of the BIIS and proxy evidence from deep water marine cores adjacent to the ice stream (Knutz et al., 2001) suggests a maximum extent reaching the shelf edge. This ice stream fed the Donegal Barra Fan (DBF), the largest glacimarine depocentre of the BIIS (Fig. 1). Irish and near-shore Scottish waters provide most of the direct evidence for glaciation of the Malin Shelf, with the majority of the shelf remaining unmapped. There, streamlined bedforms and over-deepened troughs provide evidence of grounded, fast-flowing ice that streamed south-westwards from the Inner Hebrides and then westwards around the Outer Hebrides across the shelf (Howe et al., 2012; Dove et al., 2015). Undated moraine complexes at the shelf edge mark the western limit of the BFIS (Selby, 1989; Dunlop et al., 2010). A series of smaller recessional moraines step back eastwards and become increasingly abundant on the inner shelf, marking the pattern and direction of retreating ice (Dunlop et al., 2010; Dove et al., 2015; Small et al., 2016). Dating control for the timing of advance and retreat of the BFIS relies on ice rafted debris (IRD) records. These records suggest that ice extended onto the Malin Shelf by 29 ka BP (Scourse et al., 2009) with grounded ice reaching the shelf edge by ~27 ka BP (Wilson et al., 2002; Peck et al., 2006; Scourse et al., 2009). A marked reduction in IRD flux to the DBF at 23 ka BP potentially represents the onset of deglaciation for this sector of the BIIS margin. Recent terrestrial cosmogenic nuclide (TCN) dating on Tiree constrains deglaciation of much of the mid and outer sector of the BFIS to 20.6 ± 1.2 ka and complete deglaciation of the inner sector to between 20.6 ± 1.2 and 17.5 ± 1.0 ka (Small et al., 2017).

Here, we combine new geophysical, sedimentary and radiocarbon data from across the Malin Shelf to reconstruct, for the first time, the deglacial history of the BFIS at and after the LGM. The aims of this paper are threefold: 1. to describe the glacial geomorphology, seismic stratigraphy, the lithology and geochronology of glacial sediments on the Malin Shelf; 2. to reconstruct spatially and temporally the BFIS at its maximum extent and during its retreat across the Malin Shelf, and 3. to discuss the underlying controls of BFIS dynamics in the wider context of the stability of the former BIIS.

2. Regional setting and background

The Malin Sea, known also as the Malin Shelf (Fig. 1), describes the continental shelf north of Ireland and west of Scotland, and is adjacent to a major flow pathway for Atlantic Ocean circulation (Ellett., 1979). The Slope Current transports warm saline Atlantic waters northwards around 500 m water depth (Dooley and Crease, 1978). Not always confined to the continental slope, today these waters also inundate the continental shelf along the northwest

coast of Scotland, including the Malin Shelf (Huthnance, 1986; Reid et al., 1997). Troughs and basins bounded by the SW-NE orientated Caledonian fault system extend and interlink from the Sea of Hebrides to the mid-shelf and were major flow paths for streaming ice across the Malin Shelf (Davies et al., 1984; Dobson and Whittington, 1992). Two basins, the Malin Deep in the south and a basin in the north, are separated by a central bedrock high, the Stanton Banks (Dobson and Whittington, 1992, Fig. 1).

2.1. Previous work on the glacial history of the Malin Shelf

Glaciation of the continental shelf to the shelf edge did not occur until the mid-Pleistocene, ~440 ka (Stoker et al., 1993), with localised ice extending to the shelf edge during two further glaciations in Marine Isotope Stage (MIS) 4-2 and likely including the LGM (Stoker et al., 1993). Ice draining western Scotland, the North Channel and northwest Ireland likely merged with Hebridean ice to form the BFIS (Dunlop et al., 2010; Howe et al., 2012; Finlayson et al., 2014; Dove et al., 2015), possibly reaching a shelf edge position at ~27 ka BP (Wilson et al., 2002; Peck et al., 2006; Scourse et al., 2009). The sea floor geomorphology (Dunlop et al., 2010; Finlayson et al., 2014; Dove et al., 2015) provide prima facie evidence for ice streaming (e.g. elongated bedforms, convergent flows) in this sector of the BIIS. Initial retreat was likely rapid given prevalence of over deepened troughs (Dunlop et al., 2010; Dove et al., 2015), with potentially slower, more episodic retreat on the inner shelf (Dove et al., 2015) accompanied by substantial reorganisation of ice flow directions (Finlayson et al., 2014). Iceberg furrow marks on the outer shelf, west of the Malin Deep, indicate that calving accompanied the initial retreat phase (Dunlop et al., 2010). Equivalent evidence for calving is lacking for the inner shelf, which is likely a function of deeper water in the Malin Deep and burial by post-glacial sediment further east (Dunlop et al., 2010). Sea-level studies (e.g. Brooks et al., 2008; Bradley et al., 2011) suggest that the Malin Shelf region retained a calving margin throughout deglaciation, which is supported by uninterrupted IRD flux into the DBF to 16 ka BP (Kroon et al., 2000).

There is no existing geochronology from the outer and mid Malin Shelf to constrain the glacial/deglacial chronology of the BFIS. However, there is limited chronological control for the adjacent Outer Hebrides Ice Cap. Glacimarine sediments from the Hebridean Shelf, dated to 26.4 ka (Hedges et al., 1988), provides either a minimum date for the retreat of ice from the shelf edge or it merely dates some glacimarine sediment distant to a more restricted maximum ice extent (Peacock et al., 1992). Dating of marine material from the mid-Hebridean Shelf suggests that ice did not retreat from the mid-shelf until after 18.5 ka (Peacock et al., 1992). TCN and radiocarbon ages from the eastern periphery of the Malin Sea indicates that initial deglaciation occurred before 20 ka (McCabe and Clark, 2003; Clark et al., 2009; Small et al., 2017), earlier than expected from the limited radiocarbon dates collected offshore and suggestive of a more rapid pattern of retreat across the Malin Shelf. In summary, the BFIS deglacial chronology for the outer and mid Malin Shelf is limited and a more comprehensive dataset is needed to test hypothesised patterns, styles and rates of ice marginal retreat.

3. Methodology

Cruise JC106 of the RRS James Cook in August 2014 collected sub-bottom profiler (chirp) data and sediment cores (Fig. 1). Chirp data were collected using a hull mounted Kongsberg SBP 120 sub-bottom profiler that operated a sweep frequency between 2500 and 6500 kHz, with a depth resolution of 0.3 ms. The profiles were interpreted using the IHS Kingdom™ software. To convert the two-

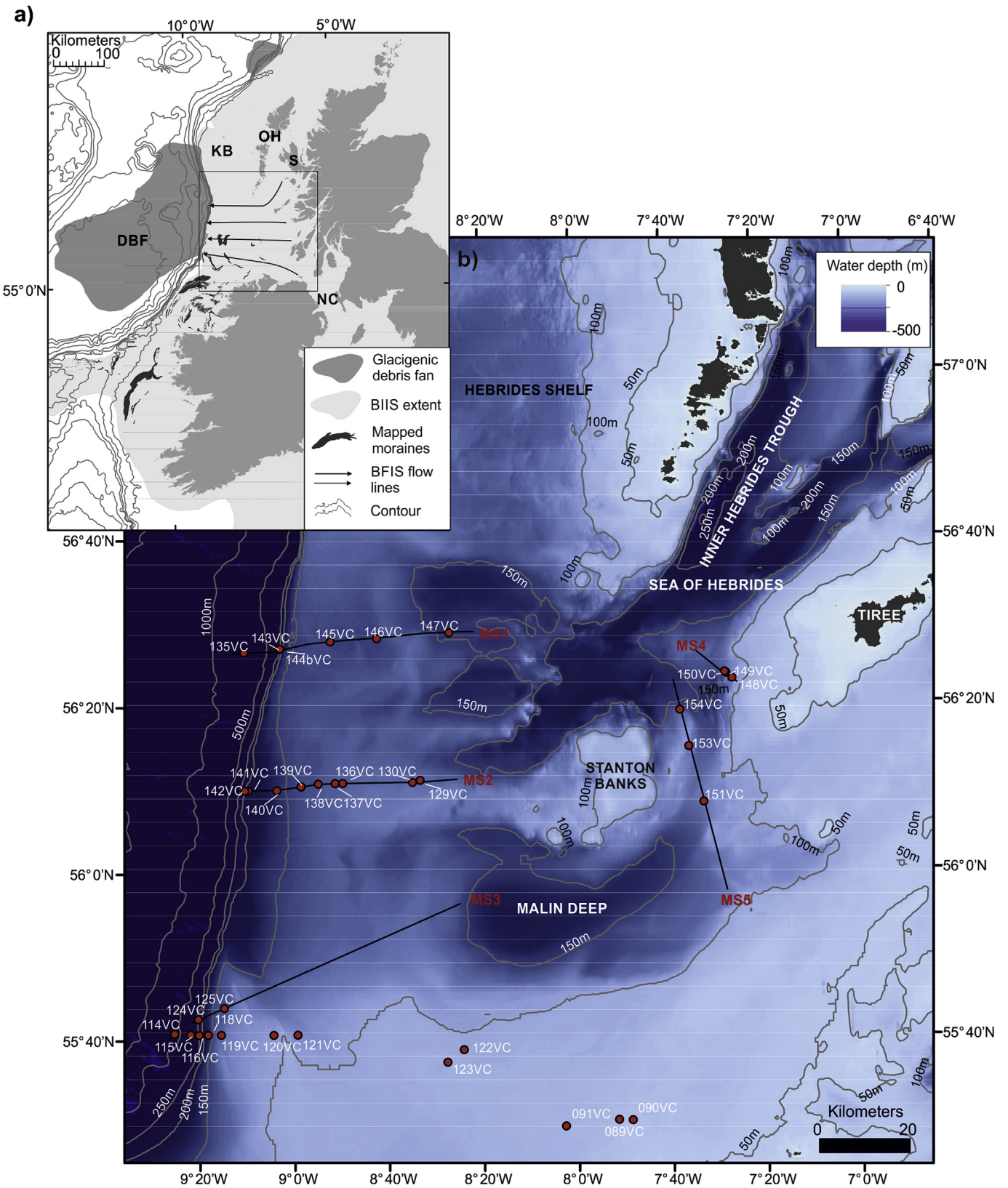


Fig. 1. (a) Regional schematic map showing the maximum extent of the British Irish Ice Sheet during the last glacial, modified from Peters et al. (2015) with the proposed flow-line directions of the major ice streams with ice-marginal and Donegal Barra Fan positions previously published by Benetti et al. (2010), Dunlop et al. (2010) Ó Cofaigh et al. (2012), Sacchetti et al. (2012) and Clark et al. (2017) and locations mentioned in the text (OH: Outer Hebrides, KB: St Kilda Basin, S: Skye, NC: North Channel, DBF: Donegal Barra Fan); Black box marks the study area; (b) The Malin Sea continental shelf showing the labelled core locations (red circles) and seismic profiles shown in Fig. 3 and 4 (black lines labelled MS1–MS5). (For interpretation of the references to colour in this figure legend, the reader is referred to the Web version of this article.)

way travel time to depth estimates an average p-wave velocity of 1620 ms^{-1} , measure from sediment cores using a Multi-Sensor Core Logger (MSCL) was used. We identify eight acoustic facies (AFA-AFH) from the sub-bottom profiler data (Fig. 2), and present five regional acoustic profiles from the outer (MS1-3, Fig. 3) and inner Malin Sea (MS4-5, Fig. 4).

Thirty-six vibrocores were retrieved (Table 1) using the British Geological Society vibrocorer with a 6 m barrel and 8 cm core diameter. The underwater position of each core was collected

using a Sonardyne Ranger USBL beacon attached to the vibrocorer. The on-board GEOTEK MSCL measured the gamma density, p-wave velocity and magnetic susceptibility of each core at two centimetre resolution. All cores were described visually, noting the lithology, texture, contacts, sedimentary structures and Munsell colour, and shear vane measurements were made using a hand held Torvane at 10 cm intervals. A GEOTEK XCT scanner provided X-radiographs at a $92 \mu\text{m}$ resolution to further refine the core lithofacies and to count the clasts larger than

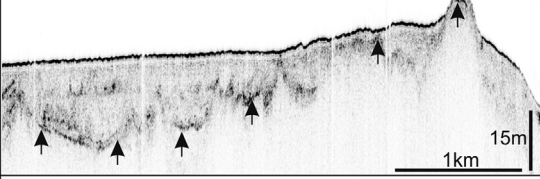
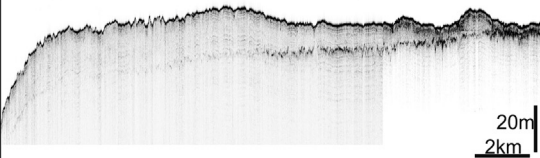
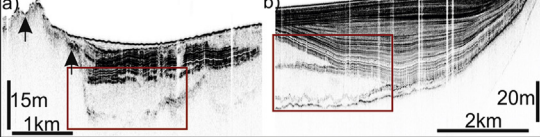
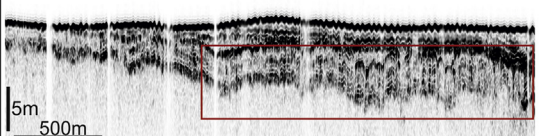
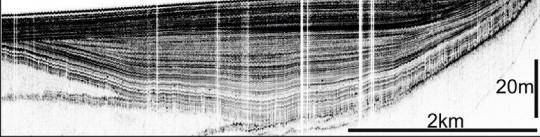
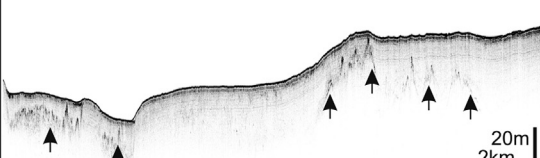
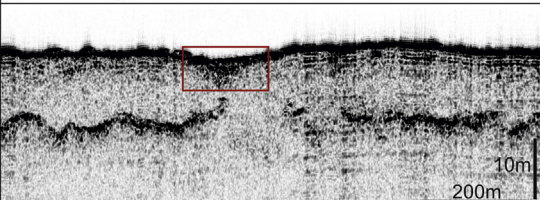
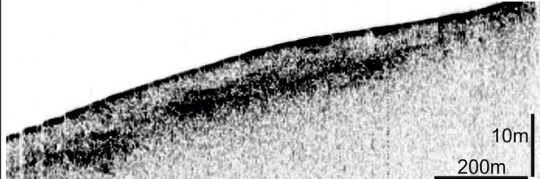
Acoustic Facies	Example	Description	Interpretation
AFA		Basal reflector that is smooth to rugged (see arrowed reflector in AFC and AFF below) and is acoustically structureless below this reflector.	Bedrock
AFB		Strong upper reflector. Internally transparent to faintly stratified. Ranges in morphology and includes large ridges, small mounds, asymmetric wedges and stacked sheets.	Moraines and grounding zone wedges that mark ice marginal positions
AFC		Internally acoustically transparent lenses (a) or wedges (b) geometries with weak boundary reflectors.	Debris flows
AFD		Chaotic to contorted internal acoustic stratification. Upper surface hummocky to truncated. Tends to directly overlie AFB.	Ice proximal glacial marine sediments containing a large IRD component. Possibly contorted by an oscillating ice margin nearby.
AFE		Acoustically stratified facies with continuous parallel reflectors. Often contains a stacked sequence of stratified units that truncate the underlying unit.	Ice distal glacial marine basin infills.
AFF		Acoustically semi-transparent facies, forming a conformable drape. Forms the uppermost acoustic facies across the study area.	Post-glacial sand and mud, likely deposited during the Holocene.
AFG		Discrete v-shaped cut and fill geometries restricted to the surface of AFB	Iceberg furrows that have been subsequently infilled by younger sediment.
AFH		Stacked lenses of internal structureless facies with some point-source diffracted hyperbole. Occurrence restricted to the upper continental shelf.	Glacigenic debris flows.

Fig. 2. Acoustic facies examples identified in the sub-bottom profile data on the Malin Shelf and upper continental slope.

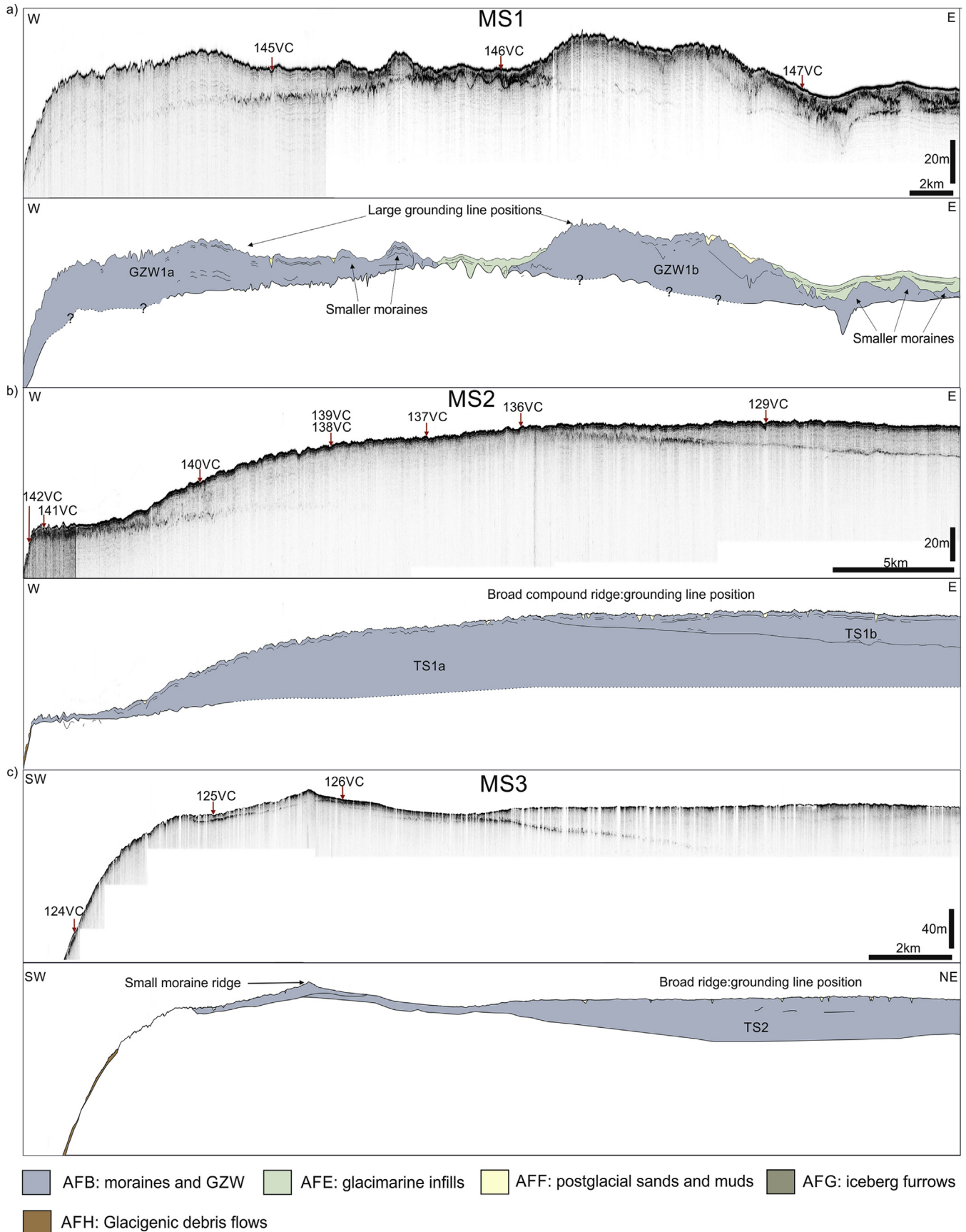


Fig. 3. Acoustic profiles of MS1-MS3 with schematic illustration of each acoustic profile below the original data where a) is MS1, b) MS2 and c) MS3. Note the different scales used for each seismic profile. Core locations are marked with a red circle. (For interpretation of the references to colour in this figure legend, the reader is referred to the Web version of this article.)

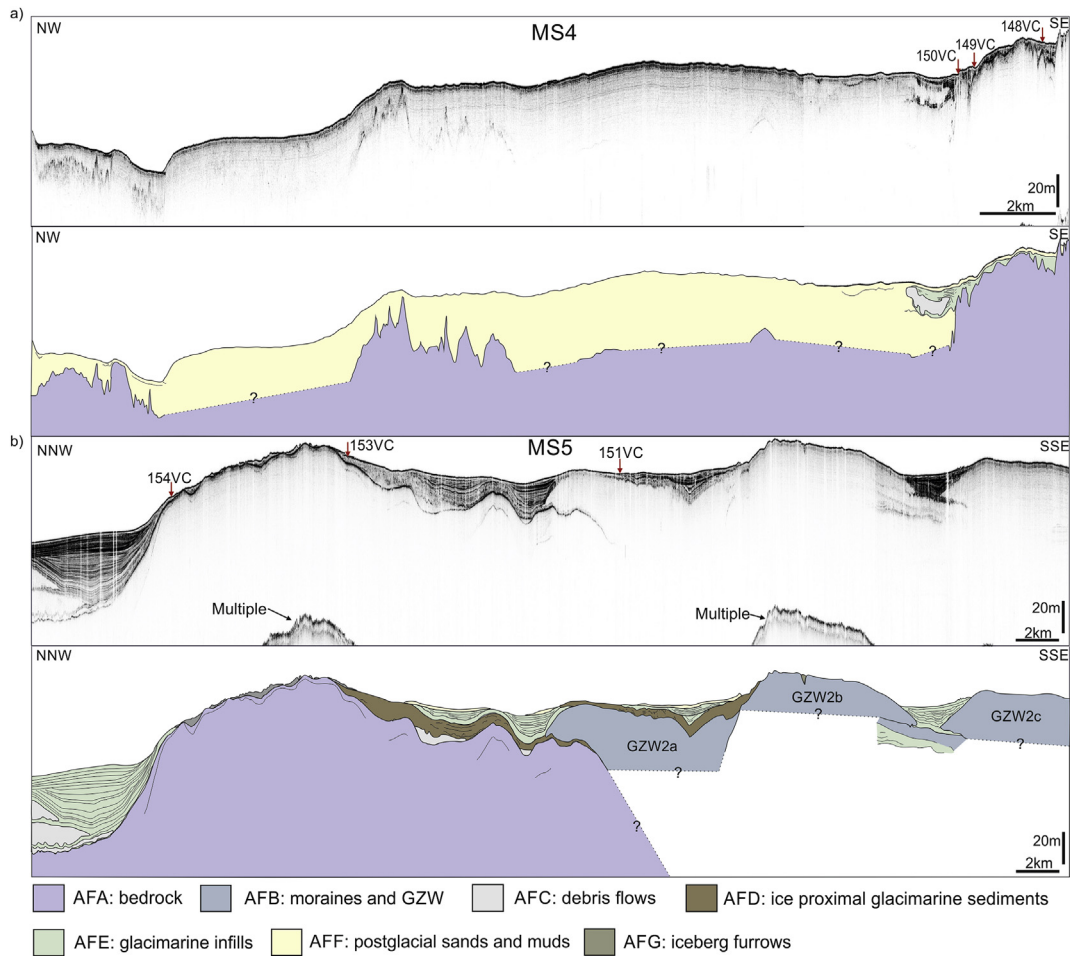


Fig. 4. Acoustic profiles of MS4–MS5 with schematic illustration of each acoustic profile below the original data where a) is MS4, b) MS5. Note the different scales used for each seismic profile. Core locations are marked with a red circle. (For interpretation of the references to colour in this figure legend, the reader is referred to the Web version of this article.)

2 mm, classified as IRD, in 2 cm windows down the core. The X-radiographs, visual logs and physical properties were used to identify six lithofacies associations (LFA1–LFA6) from the shelf cores and a further five lithofacies associations from the upper continental slope cores (LFA7–LFA11). Fig. 5 shows examples of these and they are described in section 4.2. Within the lithofacies associations, 20 individual lithofacies were identified (Table 3: after Eyles et al., 1983).

From the cores a mixture of paired bivalves, mixed benthic foraminifera samples and shell fragments were collected and cleaned for dating. All dated material is assumed to have lived in a benthic and marine environment. Only whole, unabraded foraminifera specimens were picked from sieve (500, 180 and 63 μm) residues, with the assemblage dominated by the cold water species *Elphidium clavatum*, *Cassidulina reniforme*, *Nonionella labradorica* and *Cibicides lobatulus*. Forty-nine samples for radiocarbon dating (Table 2) were collected from cores on the shelf and upper slope and submitted to the NERC radiocarbon facility in East Kilbride where they were prepared to graphite and passed to the SUERC AMS laboratory (SUERC publication codes) or the Keck C Cycle AMS laboratory, University of California, Irvine (UCIAMS publication codes) for ^{14}C measurement. The primary aim of the dating was to constrain the timing of ice-sheet advance and retreat across the shelf. We dated 32 reworked shell fragments, one fragment per date, and two mixed benthic foraminifera

samples from the over-consolidated diamicton units. These ages constrain the onset of ice advance across the shelf and the timing of sediment reworking by icebergs when the core site was free of grounded ice. These ages are treated as a maximum age of reworking. A further 15 samples were taken from above the over-consolidated diamicton in glaci-marine sediments and constrain the timing when the core site was free from grounded ice and thus a minimum age of retreat. Their stratigraphic positions are shown Fig. 6a–e and are discussed in context with the lithofacies interpretations.

The conventional ^{14}C ages were calibrated using the Marine13 curve with an inbuilt marine reservoir correction of 400 years and a ΔR of 0 years (OxCal 4.2 software; Reimer et al., 2013). The ages are reported in the text as the calibrated 2σ median result in the form ka BP (see Table 2). The radiocarbon reservoir age in the North Atlantic is known to vary both temporally and spatial (Austin et al., 1995; Peck et al., 2006; Singarayer et al., 2008). As a sensitivity test to account for the temporal and spatial variability we have applied two further age calibrations using the ΔR +300 and +700 yrs as exemplified by Small et al. (2013a). These results are reported in Table 2. The different ΔR values have a modest impact and due to the large uncertainties on the correct ΔR to use (Wanamaker et al., 2012), and for clarity in the text, we refer only to ages calibrated with a ΔR of 0 unless otherwise stated.

Table 1
Location, water depth and core recovery of cores collected from the Malin Sea.

Core name	Location	Water depth (m)	Recovery (m)
091VC	55.4958 N, 8.0456 W	76	0.62
114VC	55.6814 N, 9.4269 W	568.6	4.42
115VC	55.6802 N, 9.3696 W	384	3.67
116VC	55.6796 N, 9.3392 W	258	2.36
118VC	55.6799 N, 9.3075 W	178	1.7
119VC	55.6800 N, 9.2613 W	131	1.32
120VC	55.6805 N, 9.0756 W	110.8	0.95
121VC	55.6808 N, 8.9909 W	114	0.6
122VC	55.6505 N, 8.4030 W	95	0.6
123VC	55.6255 N, 8.4613 W	91	1.435
124VC	55.7110 N, 9.3432 W	240	5.84
125VC	55.7337 N, 9.2515 W	129	1.08
129VC	56.1894 N, 8.5530 W	130	1.33
130VC	56.1853 N, 8.5800 W	126	0.5
131VC	56.1842 N, 8.8305 W	135	1.69
135VC	56.4447 N, 9.1864 W	783	3.38
136VC	56.1837 N, 8.8578 W	124	3.92
137VC	56.1825 N, 8.9184 W	141	0.34
138VC	56.1770 N, 8.9797 W	148.5	0.275
139VC	56.1771 N, 8.9797 W	148.8	3.67
140VC	56.1693 N, 9.0662 W	167.12	4.235
141VC	56.1683 N, 9.1694 W	190	0.61
142VC	56.1684 N, 9.1804 W	201	2.93
143VC	56.4517 N, 9.0611 W	272	3.63
144bVC	56.4521 N, 9.0562 W	243	6.08
145VC	56.4669 N, 8.8744 W	147	3.98
146VC	56.4730 N, 8.7070 W	150	4.14
147VC	56.4840 N, 8.4464 W	158	6
148VC	56.3867 N, 7.4274 W	121	5.02
149VC	56.3973 N, 7.4488 W	136	4.5
150VC	56.3997 N, 7.4537 W	140	5.27
151VC	56.1405 N, 7.5377 W	122	4.1
153VC	56.2517 N, 7.5874 W	113.5	3.35
154VC	56.3253 N, 7.6181 W	138	2.7

4. Results and interpretation

4.1. Acoustic facies

4.1.1. Acoustic facies A (AFA)

AFA lacks internal structure and forms the acoustic basement in the northeast of the study area when visible. It typically has a weak to moderate strength, impenetrable and discontinuous upper surface reflector of high amplitude. This surface reflector generally forms rugged and variable topography that occasionally crops out at the sea bed (see MS4, Fig. 4a and examples in Fig. 2). In seismic line MS5 (Fig. 4b), AFA forms a large smooth ridge that has at least 100 m of relief. The depressions on either side of this ridge are infilled with acoustic facies AFC to AFF.

4.1.2. Acoustic facies B (AFB)

AFB has a transparent to faintly stratified internal acoustic return and a very strong upper reflector. On the outer shelf this upper reflector exhibits a corrugated surface pattern with hyperbolic reflections (e.g., MS1; Fig. 3), and a smooth upper reflector surface in the inner shelf (e.g., MS5; Fig. 4). The basal reflector is moderate to diffuse in strength, smooth and occasionally undulating (e.g., on the outer shelf, seismic profile MS1; Fig. 3a), discontinuous and often obscured by the overlying AFB. AFB exhibits a range of morphologies including mounds, asymmetric wedges, ridges and sheets that reach a maximum of ca. 60 m in thickness with the larger features cropping out and locally influencing the seabed topography (Fig. 3). On the inner shelf, these ridges often interdigitate with AFE, and here the lower reflector is diffuse and either very faint or not visible.

For the outer shelf sector, in the north (MS1: Fig. 3) AFB

comprises two substantial ridges (GZW1a and GZW1b) that are 23–25 m thick and have outer edges at the shelf break and 20 km inshore of it. The inner slopes of both ridges are ornamented with smaller mounds ranging in height from between 15 and 17 m with some overlapping the adjacent fronting mound to the west. The small mounds reduce in size moving east with the easternmost mound forming a thin horizontal lens 4 km in width (Fig. 3). Further south, AFB is set slightly back from the shelf break. On MS2 (Fig. 3), AFB forms a 58-m high wedge (TS1a) extending from 3.5 to 22 km, which is buried to the east by an overlapping package of AFB (TS1b) that combine to form a broad, low-relief, ridge outlined in Fig. 7. On the southern line (MS3), AFB comprises two small ridges 1 km from the shelf break, and as with MS2, there is also a thick sheet (TS2) of AFB that lies in a depression 5 km from the shelf edge (Fig. 3) that also forms part of the broad, subdued, ridge mapped on Fig. 7. On the mid-shelf, east of the Stanton Banks and on the landward slope of the Malin Deep, AFB forms a series of distinct asymmetric, acoustically transparent wedge-like features on seismic line MIS5 (GZW2a-c; Fig. 5b). The surface topography of these asymmetric wedges is flat and smooth. Across the study area AFB was sampled in 20 cores all of which recovered a stiff shelly diamicton.

4.1.3. Acoustic facies C (AFC)

AFC is acoustically transparent with no internal reflectors. It forms isolated lenses 3–11 m thick in topographic lows of AFA and AFB (see Fig. 2). It is bounded at its surface by a smooth, undulating and weak reflector, and it often has a hummocky lower bounding reflector. This facies occasionally forms acoustically transparent wedges that interdigitate with the glacial marine basin fills of AFE.

4.1.4. Acoustic facies D (AFD)

AFD is characterised by chaotic, contorted and sub-parallel internal acoustic stratifications and hyperbolic diffractions that can be strong in amplitude. This facies forms a discontinuous drape that reaches a maximum thickness of 12 m, but is generally 3–4 m thick, and overlies topographic irregularities in AFB. The upper surface can be hummocky, but more often is flat due to truncation by the overlying facies. The upper bounding reflector ranges from diffuse to moderate strength.

4.1.5. Acoustic facies E (AFE)

AFE (Fig. 2) is acoustically well stratified and is characterised by continuous, evenly spaced, parallel to sub-parallel internal reflectors. This facies often forms an on-lapping fill (max 40 m) in the topographic lows of AFA and AFB (Fig. 4b) and also overlies and truncates AFC and AFD. On the outer shelf (MS1, Fig. 3a) and within the Inner Hebrides Trough (Fig. 4) this facies forms relatively thin drapes that contain some acoustic blanking. In the deeper basins (MS5, Fig. 4b), which lie east of the Stanton Bank and to the south of the study area, AFE comprises a series of stacked stratified units with each successive unit truncating and on-lapping the previous.

4.1.6. Acoustic facies F (AFF)

AFF (Fig. 2) is an acoustically transparent to faintly laminated drape that typically forms the uppermost facies. Characterised by a diffuse lower reflector on the outer shelf, AFF forms a very thin, continuous drape of <1 m thickness that overlies AFB and AFE. On the inner shelf this unit can be very thick (greater than 40 m thick) and directly drapes bedrock (AFA: MS4, Fig. 4a). At its thickest, no underlying facies are visible due to pulse attenuation.

4.1.7. Acoustic facies G (AFG)

AFG is characterised by disrupted and chaotic internal reflectors that are contained within small v-shaped depressions cut into the GZW diamictons (AFB: Fig. 3a).

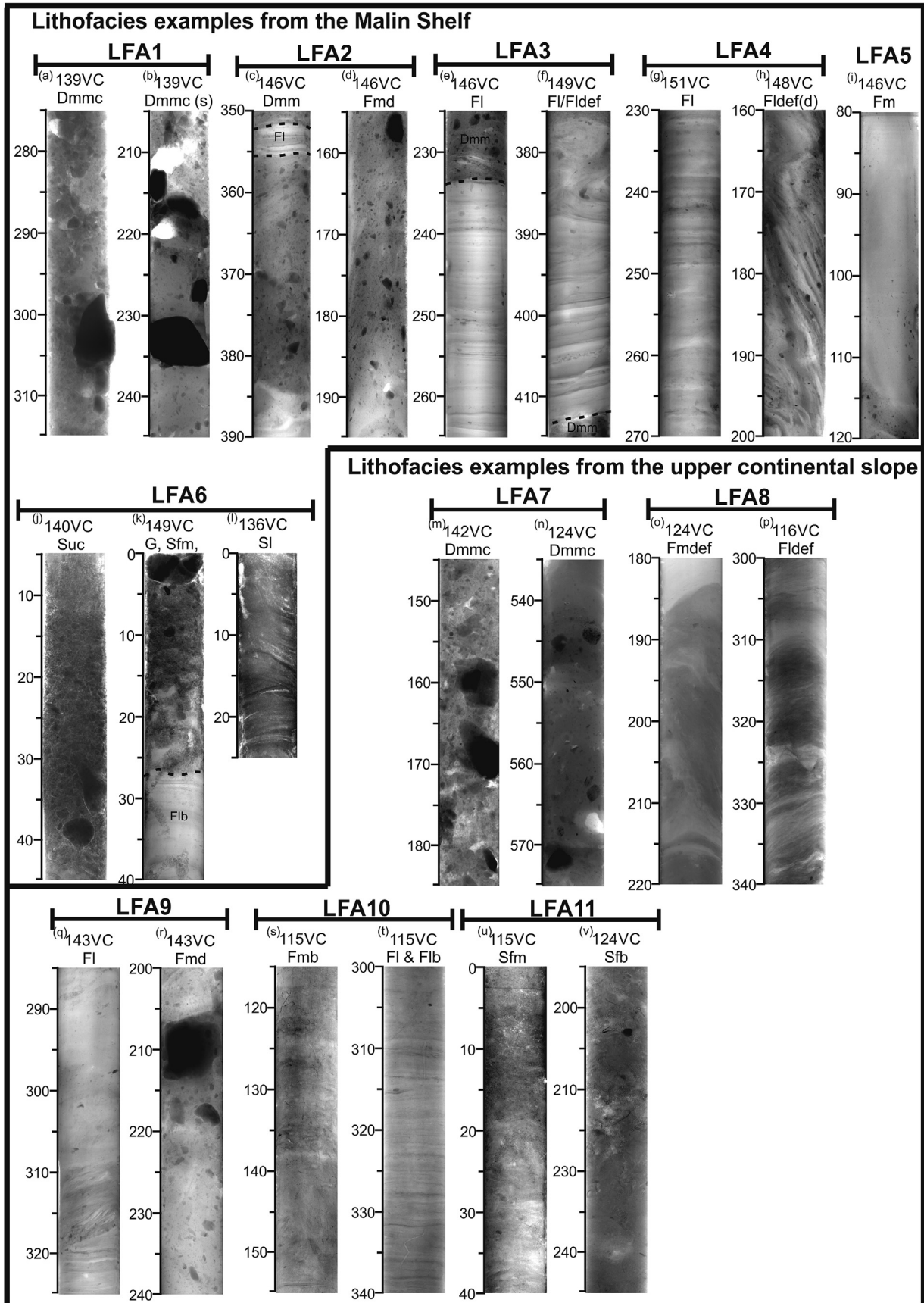


Fig. 5. Representative X-radiographs of lithofacies associations LFA1-6 and LFA7-11.

Table 2
Radiocarbon results for cores discussed in this study.

Core	Depth (cm bsf)	Sample material	$\delta^{13}\text{C}_{\text{VPDB}}\text{‰} \pm 0.1$	Carbon content (% by wt.)	^{14}C age (yrs BP)	Calibrated age range with 0 ΔR (yrs BP)	Calibrated age range with 300 ΔR (yrs BP)	Calibrated age range with 700 ΔR (yrs BP)	Laboratory code
115VC	365–367	Mixed benthic foraminifera	–1.425	13.8	19299 \pm 66	22751 \pm 229	22464 \pm 145	22058 \pm 231	SUERC-63566
116VC	140	Shell fragment	0.492	11.6	15487 \pm 41	18326 \pm 165	17981 \pm 153	17528 \pm 169	SUERC-59493
116VC	231–233	Mixed benthic foraminifera	–0.993	13.1	19299 \pm 58	22750 \pm 221	22463 \pm 133	22056 \pm 220	SUERC-63567
124VC	303–304	Shell fragment	1.233	10.7	12733 \pm 39	14312 \pm 272	13914 \pm 135	13472 \pm 125	SUERC-58376
124VC	305–307	Shell fragment	1.834	11	12675 \pm 39	14189 \pm 190	13854 \pm 129	13417 \pm 108	SUERC-58377
124VC	522–524	Mixed benthic foraminifera	–1.811	11.2	16025 \pm 44	18862 \pm 106	18598 \pm 129	18131 \pm 178	SUERC-63568
125VC	69.5	Shell fragment	1.043	11.44	11373 \pm 39	12826 \pm 129	12612 \pm 80	12042 \pm 204	SUERC-72872
125VC	115	Shell fragment	1.272	11.41	22813 \pm 61	26719 \pm 318	26310 \pm 235	25955 \pm 135	SUERC-72873
125VC	117	Shell fragment	1.007	11.52	22906 \pm 62	26825 \pm 302	26408 \pm 255	26018 \pm 147	SUERC-72874
130VC	45	Shell fragment	0.875	11.8	49782 \pm 1271	Out of range	Out of range	Out of range	SUERC-59482
136VC	232–233	Shell fragment	1.94	11.5	19854 \pm 52	23418 \pm 251	23078 \pm 249	22601 \pm 188	SUERC-58378
139VC	151–154	Mixed benthic foraminifera	–2.274	10.2	18920 \pm 80	22389 \pm 184	22082 \pm 249	21583 \pm 269	UCIAMS-176381
139VC	172	Shell fragment	1.288	11.7	50780 \pm 2520	Out of range	Out of range	Out of range	SUERC-59488
139VC	208	Bryozoa	0.123	9.1	11160 \pm 39	12662 \pm 88	12379 \pm 206	11591 \pm 267	SUERC-59489
139VC	305.5	Shell fragment	0.698	11.08	13017 \pm 39	14978 \pm 221	14276 \pm 253	13789 \pm 137	SUERC-58379
139VC	312	Shell fragments	0.878	10.6	Indistinguishable from background				SUERC-59483
139VC	331.5	Shell fragment	0.657	9	13048 \pm 38	15031 \pm 204	14345 \pm 284	13825 \pm 133	SUERC-59490
139VC	332.5	Shell fragment	1.512	10.4	11280 \pm 38	12749 \pm 114	12542 \pm 104	11866 \pm 202	SUERC-59491
139VC	348.5	Shell fragment	1.158	8.3	20397 \pm 77	24179 \pm 212	23850 \pm 225	23371 \pm 265	SUERC-59487
139VC	339	Shell fragment	0.675	10.7	12729 \pm 37	14299 \pm 263	13910 \pm 131	13467 \pm 120	SUERC-59486
139VC	Shoe	Shell fragment	0.415	11.5	13023 \pm 38	14989 \pm 216	14287 \pm 259	13796 \pm 135	SUERC-58382
142VC	150–151	Mixed benthic foraminifera	–0.647	10.9	18922 \pm 50	22402 \pm 123	22078 \pm 212	21593 \pm 216	SUERC-58325
142VC	160	Shell fragment	–0.391	9.6	50975 \pm 1485	Out of range	Out of range	Out of range	SUERC-59496
142VC	189.5	Shell fragment	–0.686	11.3	41614 \pm 474	44711 \pm 864	44443 \pm 892	44063 \pm 886	SUERC-59497
142VC	223	Shell fragment	0.857	11.74	15331 \pm 41	18138 \pm 174	17810 \pm 167	17324 \pm 188	SUERC-59498
142VC	269.5	Shell fragment	1.738	11.1	17269 \pm 51	20228 \pm 198	19983 \pm 194	19510 \pm 180	SUERC-59499
142VC	210	Shell fragment	–0.174	10.6	15496 \pm 41	18339 \pm 163	17991 \pm 153	17539 \pm 169	SUERC-59503
142VC	272	Shell fragment	0.405	11.3	Indistinguishable from background				SUERC-59500
142VC	285	Shell fragment	–0.845	11.5	Indistinguishable from background				SUERC-59501
143VC	323–325	Mixed benthic foraminifera	–0.993	11.9	15287 \pm 46	18090 \pm 174	17766 \pm 174	17271 \pm 196	SUERC-63565
143VC	330	Shell fragment	0.799	11.7	44474 \pm 689	Out of range	Out of range	Out of range	SUERC-59506
143VC	363	Shell fragment	–0.304	11.5	>53893	Out of range	Out of range	Out of range	SUERC-59508
143VC	Shoe	Shell fragment	1.321	11.8	Indistinguishable from background				SUERC-59507
144bVC	517–518	Shell fragment	0.067	11.6	Indistinguishable from background				SUERC-58383
145VC	256–257	Shell fragment	0.07	11.5	15431 \pm 41	18251 \pm 169	17919 \pm 155	17455 \pm 174	SUERC-58384
145VC	318–320	Shell fragment	0.196	10.4	18423 \pm 51	21824 \pm 196	21450 \pm 233	20886 \pm 202	SUERC-58385

Table 2 (continued)

Core	Depth (cm bsf)	Sample material	$\delta^{13}\text{C}_{\text{VPDB}}\text{‰} \pm 0.1$	Carbon content (% by wt.)	^{14}C age (yrs BP)	Calibrated age range with 0 ΔR (yrs BP)	Calibrated age range with 300 ΔR (yrs BP)	Calibrated age range with 700 ΔR (yrs BP)	Laboratory code
146VC	223	Mixed benthic foraminifera	-7.491	9.8	20200 \pm 80	23828 \pm 251	23478 \pm 288	23007 \pm 290	UCIAMS-176382
146VC	225	Mixed benthic foraminifera	-3.325	10.5	22030 \pm 100	25897 \pm 178	25662 \pm 225	25265 \pm 302	UCIAMS-176383
146VC	369	Mixed benthic foraminifera	5.401	10.6	20730 \pm 100	24424 \pm 331	24089 \pm 270	23646 \pm 300	UCIAMS-164440
146VC	389	Mixed benthic foraminifera	2.942	11.8	Indistinguishable from background				SUERC-58386
147VC	293	Shell fragment	0.986	10.64	Indistinguishable from background				SUERC-72875
147VC	422	Shell fragment	5.507	11.91	Indistinguishable from background				UCIAMS-186925
147VC	449	Shell fragment	1.245	10.78	>49150	Out of range	Out of range	Out of range	SUERC-72876
147VC	489	Shell fragment	3.24	7.37	Indistinguishable from background				UCIAMS-186923
149VC	421	Shell fragment	-0.491	11.8	17155 \pm 47	20204 \pm 190	19846 \pm 202	19375 \pm 180	SUERC-59509
151VC	300	Yodiella sp	0.194	11.3	14320 \pm 41	16860 \pm 221	16411 \pm 200	15886 \pm 174	SUERC-67939
151VC	302	Mixed benthic foraminifera	-1.673	7.7	19690 \pm 90	23232 \pm 292	22853 \pm 286	22460 \pm 194	UCIAMS-179841
153VC	389	Mixed benthic foraminifera	1.158	16.1	19210 \pm 110	22679 \pm 270	22365 \pm 261	21956 \pm 321	UCIAMS-164432
153VC	277	Mixed benthic foraminifera	3.744	12.7	18670 \pm 90	22129 \pm 261	21757 \pm 265	21229 \pm 304	UCIAMS-164433
154VC	211	Mixed benthic foraminifera							
154VC	214	Mixed benthic foraminifera							

4.1.8. Acoustic facies H (AFH)

AFH is restricted to the upper continental slope and form a series of stacked, smooth but hummocky lenses that are internally structureless and acoustically homogeneous. AFH often contains isolated point-source diffracted hyperbole concentrated at the basal reflector.

4.1.9. Acoustic interpretation

AFA, is interpreted as bedrock and is restricted to the Inner Hebrides Trough and the ridge behind the Stanton Banks (Fig. 4a and b). Elsewhere the Malin Sea shelf contains very thick sequences of Quaternary sediments that overlie and obscure the bedrock (AFA) in the seismic data (Stoker et al., 1993; Fyfe et al., 1993).

AFB is interpreted as a sub-glacial till that has been formed into a series of grounding-zone wedges (GZWs), till sheets and moraines marking the grounding line positions of the BFIS at the shelf edge and during subsequent retreat. These ice-marginal features identified in the seismic lines have a strong signature in the bathymetric data (Fig. 7), but previous descriptions were restricted to the south of the study area (Dunlop et al., 2010). Together, these data identify two sets of grounding line positions, separated by two deep troughs (~170 m-bsl). The outer shelf is characterised by a series of small moraines, GZWs (GWZ1a-b) and broad subdued wedges interpreted as till sheets (TS1-2) that combine to form the broad sediment ridge mapped in Fig. 7. This marks a grounding line position that extends the width of the Malin Shelf. No GZWs or moraines were visible in the seismic or bathymetry data from the deep troughs. Directly east of the Stanton Banks, a second set of GZWs (2a-c) are also visible in the bathymetry data and were mapped in part by Dunlop et al. (2010). The morphology of the Malin Shelf features is consistent with GZWs described from other glaciated margins (e.g., Batchelor and Dowdeswell, 2015; Anderson and Jakobsson, 2016; Evans and Hogan, 2016). These features form subdued features on the Malin Shelf, wide relative to their height. The size and morphology of these wedges are characteristic of a grounding zone where the thickness of the GZW is constrained by

the sub-ice shelf cavity as opposed to moraine ridges formed at a grounded tidewater cliff (Dowdeswell and Fugelli, 2012). The smaller mounds located on the edge of the large GZWs in seismic line MS1 (Fig. 3a) are likely moraine banks produced by minor ice stream re-advances during a period of prolonged retreat (Batchelor and Dowdeswell, 2015).

AFC is consistent with an interpretation of as debris flows (e.g. Dowdeswell et al., 2010; Batchelor et al., 2011). AFC was not sampled during the coring.

AFD was captured in two cores (150VC and 153VC), both containing a massive, soft, pebbly rich mud. Thus, AFD is interpreted as an ice proximal, IRD-rich deposit. The contorted internal structure may represent modification of the sediment from either post-deposition settling or minor oscillation of the ice margin near to

Table 3

Lithofacies identified in the cores from the Malin Sea (After Eyles et al., 1983).

Lithofacies	Description
Dmm	Diamict, matrix supported and massive
Dmmc	Diamict, matrix supported, consolidated (>40 kPa)
Dms	Diamict, matrix supported and stratified
Gm	Gravel, clast supported and massive
Gms	Gravel, matrix supported
Sfm	Muddy fine sand, massive
Sm	Sand, massive
Smg	Sand, massive with some gravel
Ss	Sand, stratified
Sl	Sand, laminated
Suf	Sand, upward fining
Fm	Mud/muddy sand, massive
Fmd	Mud/muddy sand, with clast
Fmb	Mud/muddy sand, with bioturbation
Fmg	Mud/muddy sand, massive with gravel
Fs	Mud/muddy sand, stratified
Fsb	Mud/muddy sand, stratified with bioturbation
Fl	Mud/muddy sand, laminated
Fldef	Mud/muddy sand, deformed laminations
Flb	Mud/muddy sand, laminated with bioturbation

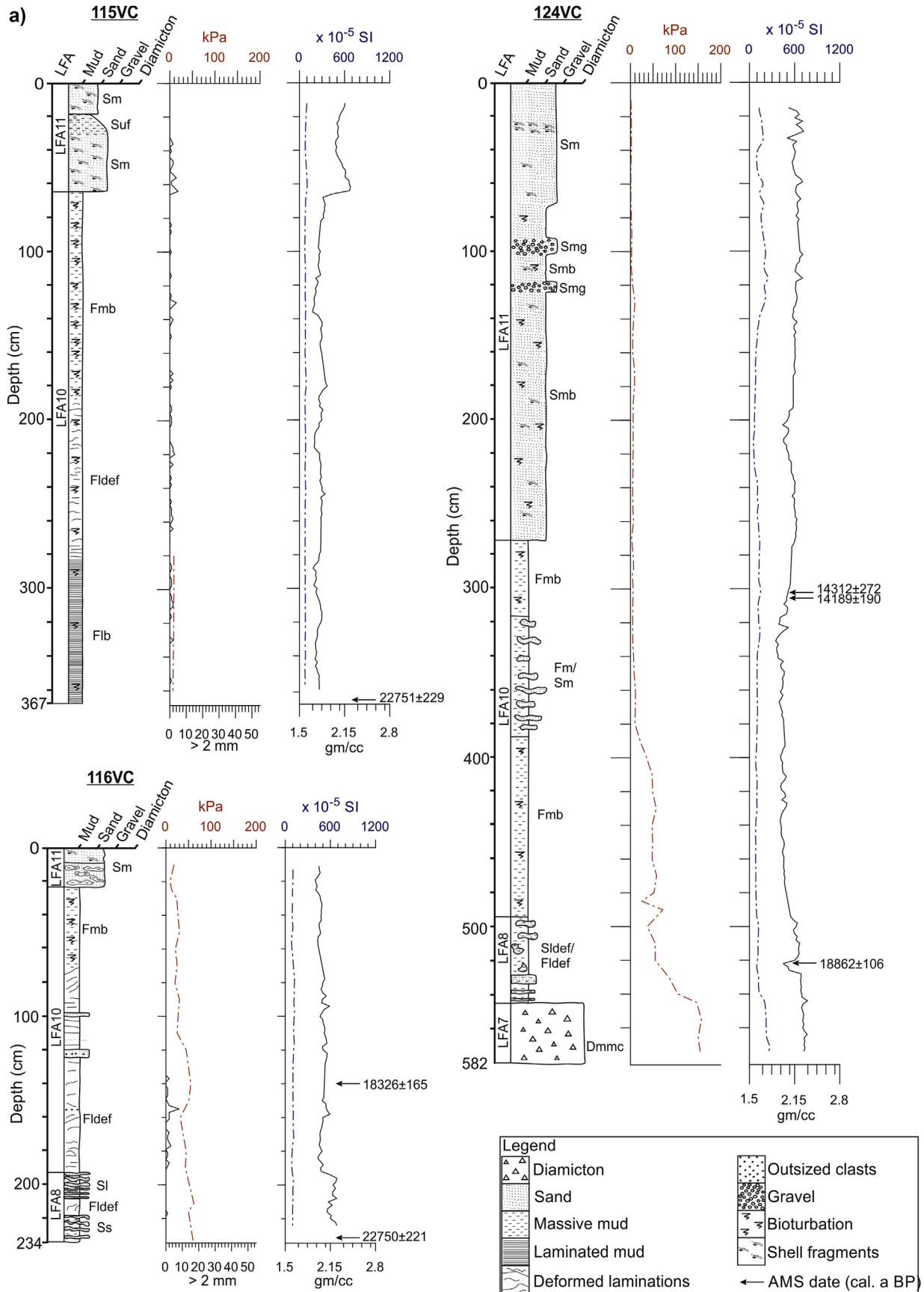


Fig. 6. Core logs of key cores mentioned in the text where a) cores located on MS3, b) cores located on MS2, c) cores located on MS1, d) cores located on MS4, e) cores located on MS5. Shear strength measurements, >2 mm clast counts, magnetic susceptibility and bulk density results are added to these logs along with the median radiocarbon ages.

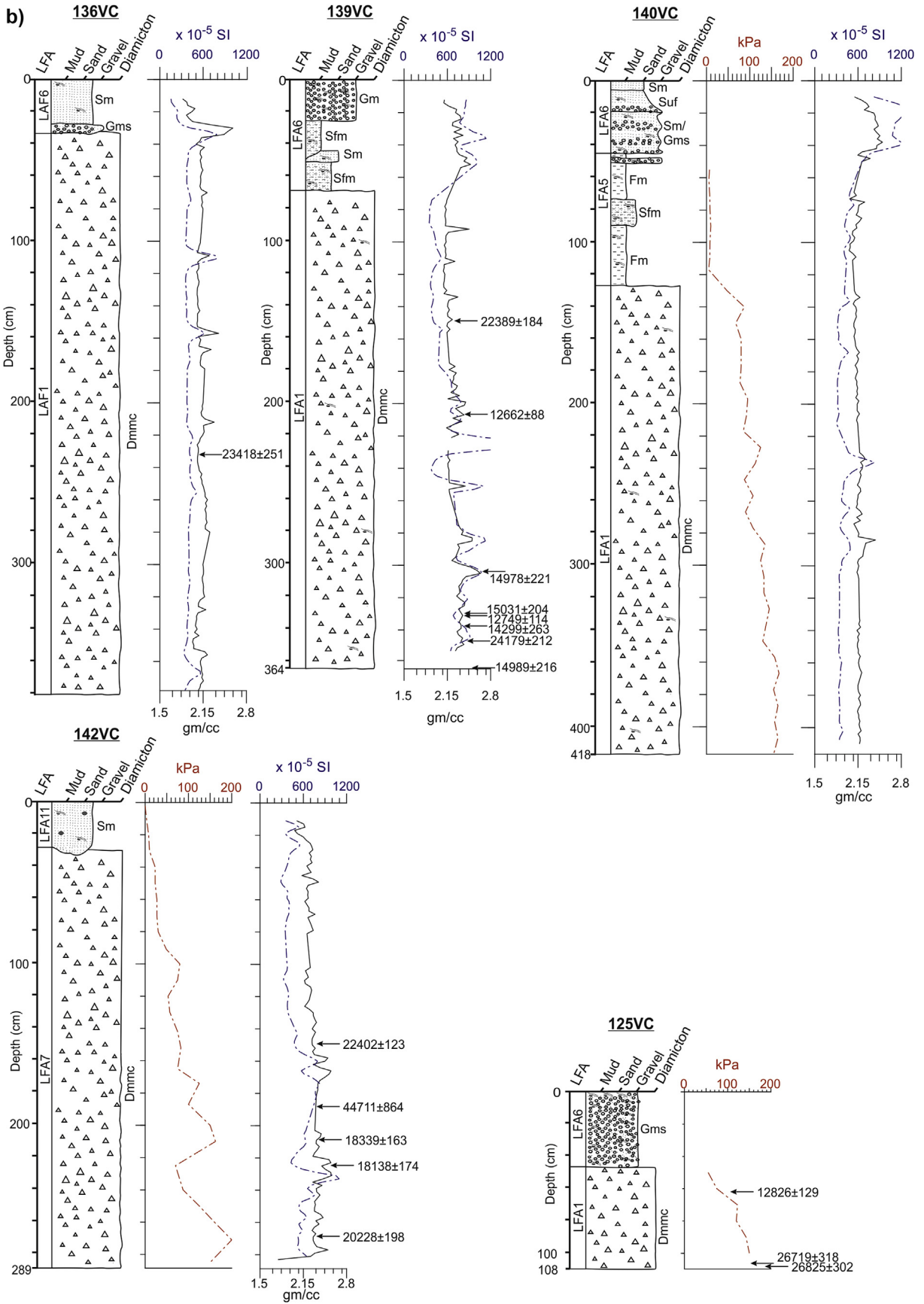


Fig. 6. (continued).

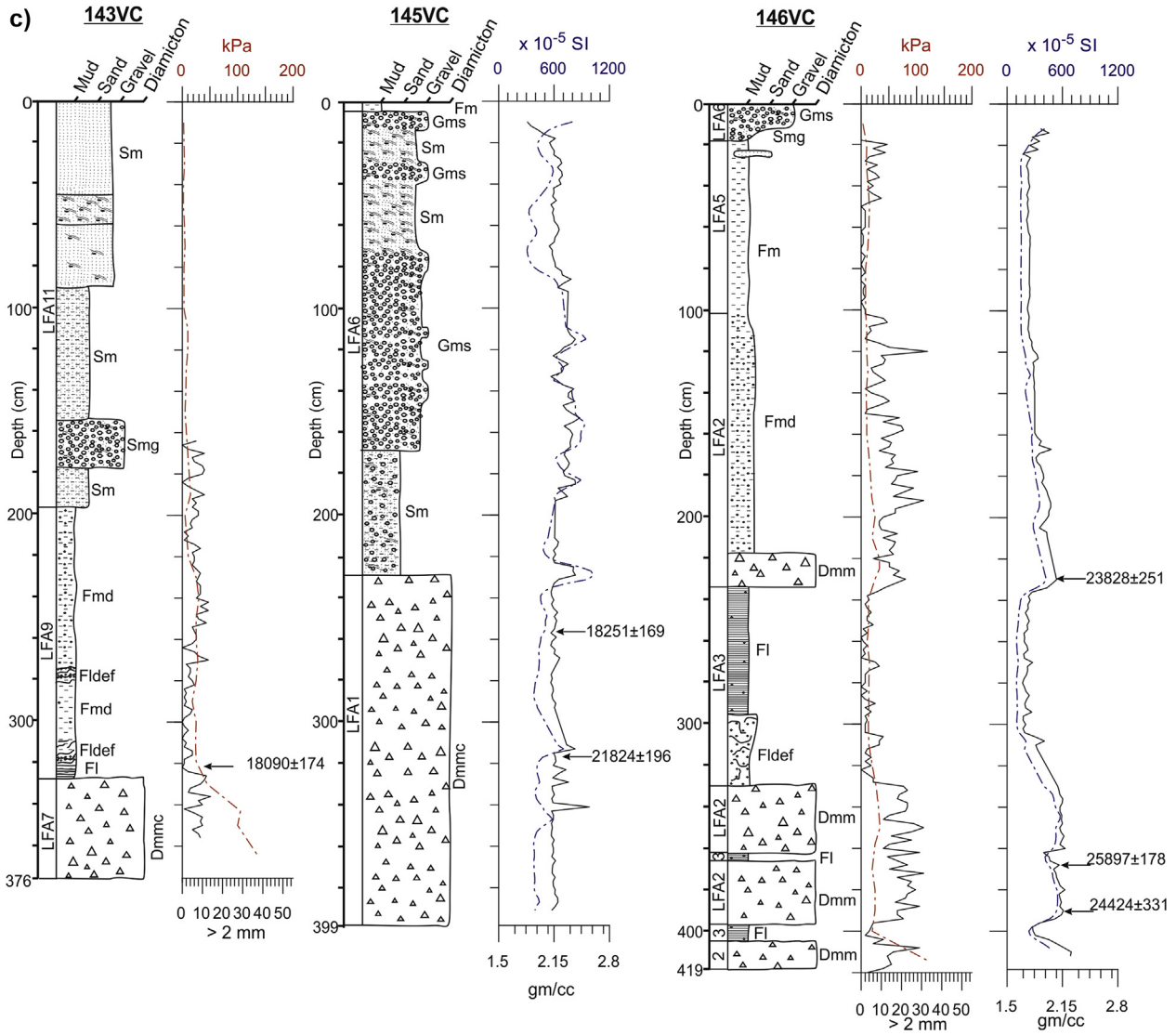


Fig. 6. (continued).

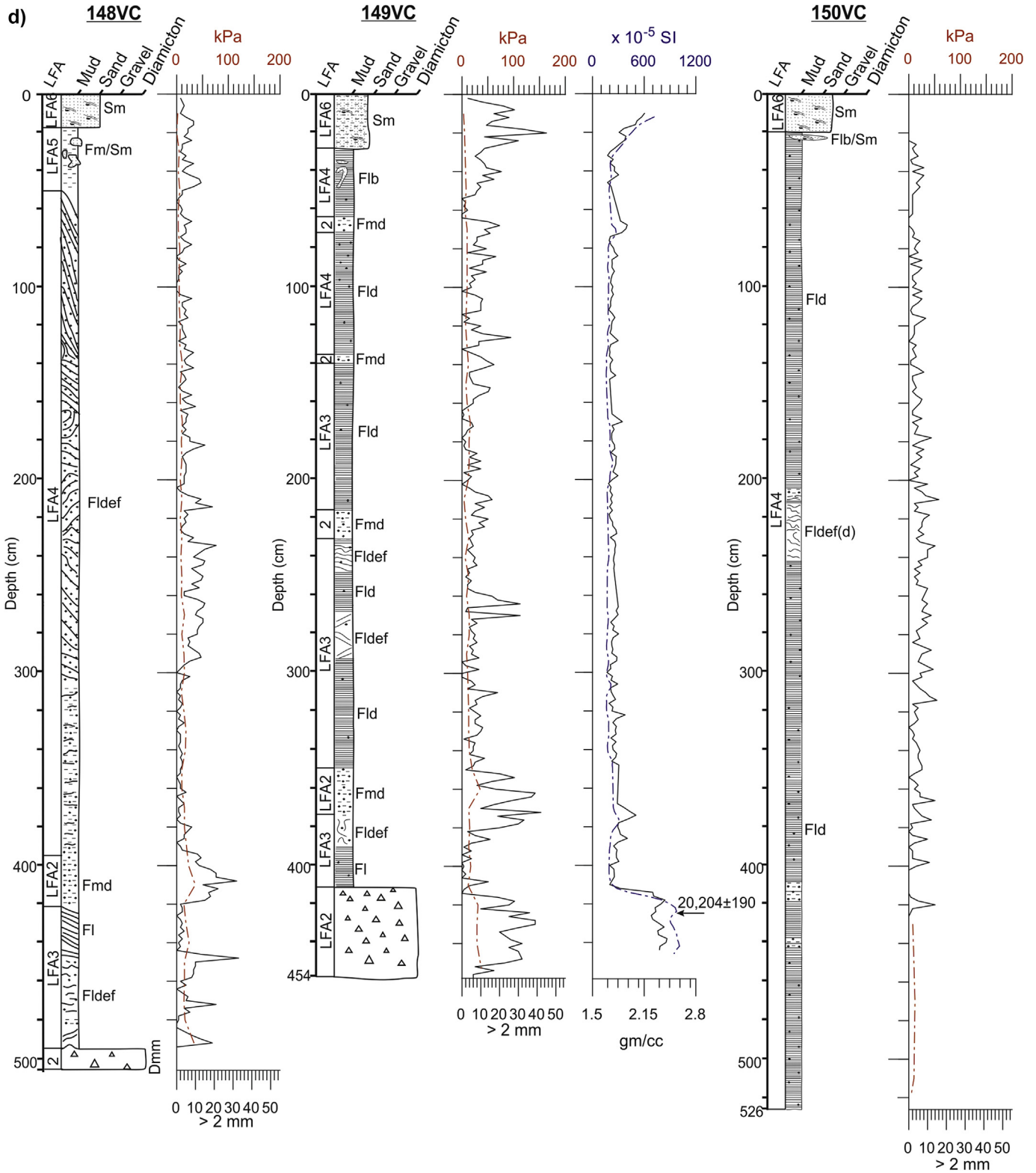


Fig. 6. (continued).

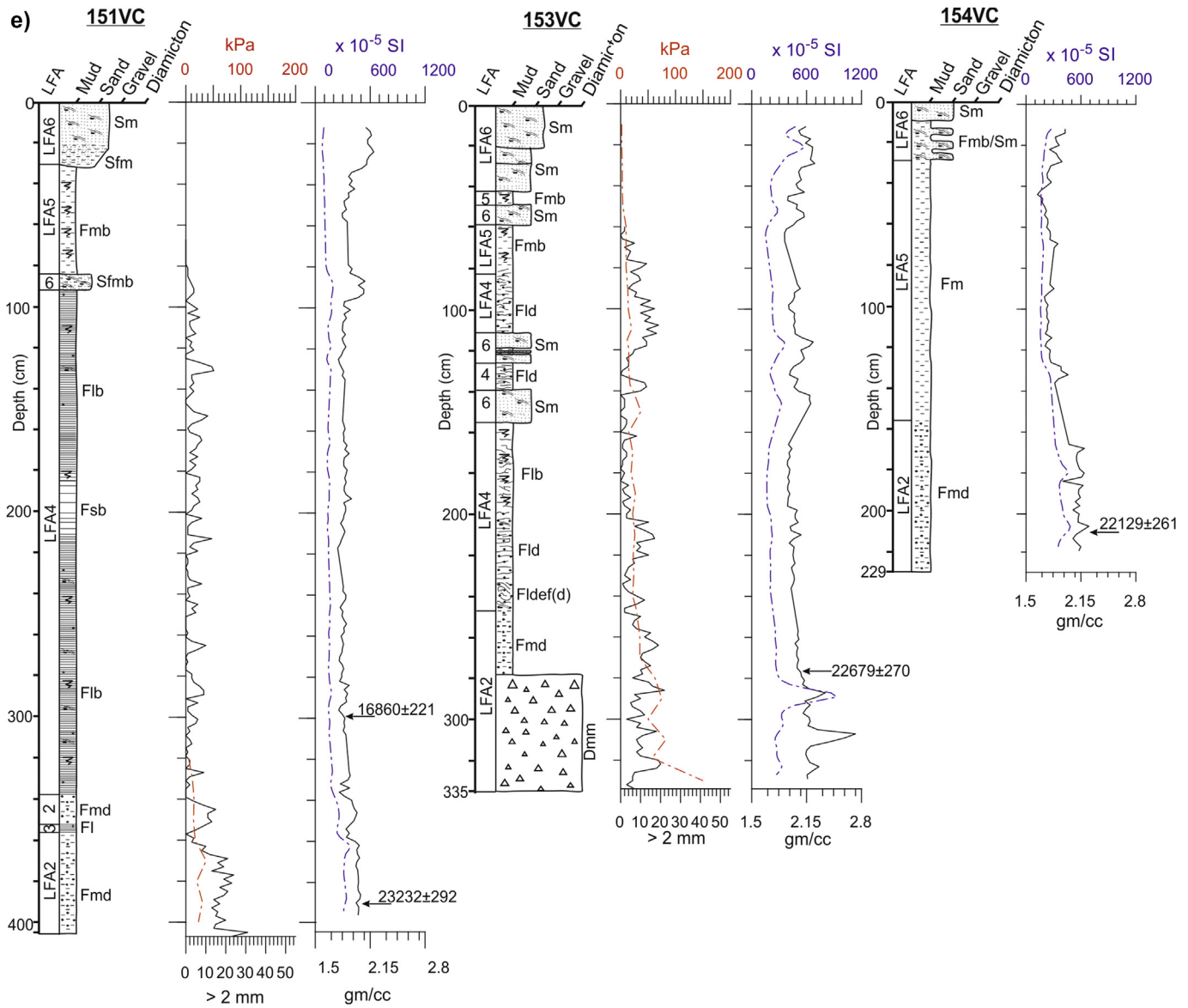


Fig. 6. (continued).

the area of sediment deposition. The hyperbolic diffractions are likely caused by the presence of clasts, that are either large or occur in high concentrations.

AFE is interpreted as glaci-marine basin fills that are more distal to the ice margin. Winkelmann et al. (2008) suggest that this type of stratification could be a result of changing clast concentrations relating to variations in IRD and suspension dominated depositional processes. AFE was sampled in eight cores that contained alternating massive pebbly rich mud with laminated silts and clays. Similar acoustic facies and lithofacies are documented in the Arctic (e.g., Dowdeswell et al., 2010; Batchelor et al., 2011; Hogan et al., 2016). The stratification is often conformable in the sub-bottom profile data, consistent with suspension settling from turbid meltwater plumes and IRD rainout (Hogan et al., 2012; Ó Cofaigh et al., 2016). In MS5 (Fig. 4) there is evidence of truncation of the acoustically stratified sediment and the presence of transparent wedges (AFC) within AFE. This is consistent with downslope remobilisation and erosional events characteristic of these glaci-marine settings (c.f., Ó Cofaigh et al., 2016).

AFF was captured in nearly all the cores collected in this study

and comprised coarse-grained sand to gravel or shell hash. On the inner Malin Shelf and in the Inner Hebrides Trough AFF consists of medium, fine or muddy-fine sand. The abundance of shell hash and whole shells, the coarse sand and gravels combined with the stratigraphy is consistent with post-glacial bottom-current winnowing (Howe et al., 2012).

AFG is interpreted as furrow infill, with the furrows formed by sea-bed scour by the keels of floating icebergs calved from the BFIS. Dunlop et al. (2010) noted that the outer Malin shelf bathymetry in particular contains high concentrations of v-shaped elongated furrows down to ca. 190 m water depth. The furrow infill (Core 145VC) consisted of coarse sandy-gravel overlying a stiff diamicton (Fig. 6c).

AFH is interpreted as the deposits of glaciogenic debris flows on the continental slope likely sourced when BFIS ice was at the shelf edge or by postglacial downslope mobilisation or iceberg disturbance. The stacked lenses are characteristic of episodic subaqueous glaciogenic debris flows and gravity deposits sourced from ice streams crossing the continental shelf (e.g. Laberg and Vorren, 1995; Elverhøi et al., 1997). AFH was recovered in three cores

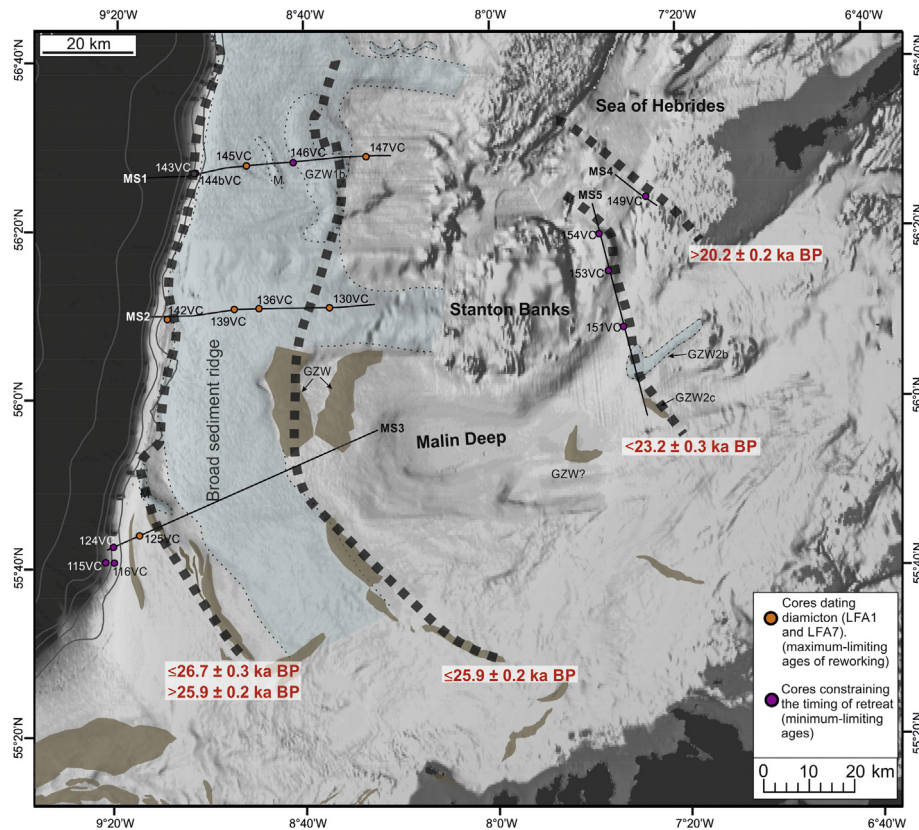


Fig. 7. Greyscale hillshade image of the Malin Sea shelf, with previously published glacial geomorphology shaded in brown (Dunlop and Benetti) and new features identified by the author, and ground truthed using acoustic sub-bottom profiles and core data, in blue. The location of the seismic lines shown in Figs. 3–4 and the cores used to constrain the chronology of the BFIS are also added, along with proposed isochrones (dashed black lines) of the BFIS margins. Source of hillshade image from EMODnet Bathymetry portal (www.emodnet-bathymetry.eu). (For interpretation of the references to colour in this figure legend, the reader is referred to the Web version of this article.)

(124VC, 142VC and 143VC) and consists of a stiff basal diamicton representing the debris flows overlain by laminated silts and clays, massive pebbly mud and/or massive bioturbated muds that represents the transition to an ice distal setting once ice had retreated from the shelf edge.

4.2. Sedimentology

4.2.1. Shelf lithofacies associations (LFA1–LFA4)

4.2.1.1. LFA1: stiff diamicton (Dmmc, Dms). The basal lithofacies of 19 cores on the shelf and particularly the outer shelf are highly consolidated diamicton (Dmmc) comprising predominantly massive, dark grey (Munsell colour 5Y4-1), matrix-supported sub-rounded to sub-angular gravel to pebble-sized clasts in a silty-clay to sandy-silt matrix. Shell fragments are frequent to rare, and when present they are typically highly abraded although occasionally are in a good condition. In some cores LFA1 contains internal structures such as sand lenses (1–2 cm thick), crude stratification (Dms), dewatering structures and preferential clast alignments that are evident only in the X-radiographs (Fig. 5). LFA1 is typically over-consolidated with shear strengths averaging 100 kPa, varying between 45 and 200 kPa, and increasing with depth. LFA1 has high wet bulk densities and magnetic susceptibilities (Fig. 6). LFA1 is constrained by 25 radiocarbon ages (Table 2), twelve of which are finite. These ages are not in stratigraphical order within individual cores reflecting the prevalence of reworking and mixing in the sedimentary processes (Fig. 6). The oldest ages, 26719 ± 318 and 26825 ± 302 cal yrs BP, are from the shelf edge (125VC), with a further five ages ranging between 24179 ± 212 cal yrs BP to

18251 ± 169 cal yrs BP from these outer GZWs and Till sheets (136VC, 145VC, 139VC; Table 1, Fig. 6b and c). 139VC contains most diverse set of radiocarbon ages, ranging from infinite to six measurements between $15,031 \pm 204$ cal yrs BP and $12,662 \pm 88$ cal yrs BP. The uppermost age in core 125VC, at 69.5 cm down the core also provides a young age of $12,826 \pm 129$ cal yrs BP.

4.2.1.2. LFA2: soft diamicton or massive pebbly mud (LFA2: Dmm, Dms, Fmd). LFA2 is a matrix-supported diamicton with a sandy-silt matrix and gravel to pebble size clasts (Dmm) and/or massive silts containing abundant pebble-size clasts (Fmd) present on the outer shelf (146VC, 147VC) and inner shelf (148VC, 149VC, 151VC, 153VC and 154VC) (Fig. 6d and e). These diamictons often form discrete beds (6–55 cm thick) and can repeat 2 to 5 times in a core often alternating with LFA3 laminated mud. The diamicton in LFA2 varies from massive (Dmm) to stratified (Dms) and have low shear strengths averaging 24.6 kPa with a 37 kPa maximum (149VC). The pebbly muds (Fmd) also form multiple beds ranging from 7 to 86 cm thick within individual cores, and contain fewer pebble-gravel sized clasts only visible in the X-radiographs and in a muddy-matrix that has low shear strengths of no more than 10 kPa. If present together (cores 146VC, 147VC, 148VC, 149VC, and 153VC), the Fmd is always stratigraphically higher than Dmm. The Fmd is often massive, but with occasional water escape structures and preferential near vertical grain alignment (Fig. 5). The upper and lower contacts of LFA2 are often sharp and can form intruded/loaded contacts with the underlying LFA3. Occasionally the lower boundary can be gradational over 5 cm and consist of laminated fine mud and diamicton (Fig. 5). The sediment matrix varies from

dark grey to very dark grey (5Y 4/1, 5Y 3/1) or olive brown/greyish brown (5Y 4/2, 2.5Y 5/2) with the Dmm darker in colour than the Fmd. LFA2 is characterised by medium wet bulk densities and variable high magnetic susceptibilities (Fig. 6) due to the clast content. Seven radiocarbon ages were obtained from LFA2 targeting mixed benthic foraminifera, with the three oldest ages from core 146VC on the outer shelf ($23,828 \pm 251$, $25,897 \pm 178$ and $24,424 \pm 331$ cal yrs BP; Fig. 6c) again not in stratigraphic order. A chronologically tight cluster of three radiocarbon ages come from the mid-shelf (151VC, 153VC, 154VC; $23,232 \pm 292$, $22,679 \pm 270$ and $22,129 \pm 261$ cal yrs BP, respectively), along with an additional 14C age for a shell fragment in a soft diamicton (149VC, $20,204 \pm 190$ cal yrs BP; Fig. 6d and e).

4.2.1.3. LFA3: laminated mud (Fl, Fldef). LFA3 consists of greyish brown to very dark grey (2.5Y 5/2 to 5Y 3/1) fine (1 cm to >1 mm thick) horizontal laminated clays and silt with no evidence of bioturbation, although deformation structures, including convoluted bedding, ball and pillow structures or bending of the underlying laminae, coincident with isolated dropstones, are visible. High angle conjugate to normal brittle faults are also visible and are more prevalent towards the core base. Although >2 mm clast are present in the Fl, the clast count is consistently less than 10 grains (per 2 cm window). Laminations vary from: (i) continuous horizontal to sub-horizontal laminae with sharp upper and lower contacts; to (ii) deformed, convoluted and discontinuous laminae. Basal sections of seven cores (146VC, 147VC, 148VC, 149VC, 151VC, 153VC, 154VC: Fig. 6d and e) consist of LFA3 alternating with LFA2 with sharp upper and lower contacts (Fig. 5c). Fl is firmer (shear strength average 16 kPa, range 4–34 kPa) when overlain by LFA2. Towards the upper contact of Fl the bedding often becomes deformed, with convoluted structures (Fldef).

4.2.1.4. LFA4: laminated, stratified and bioturbated mud containing frequent clasts (Fld, Flb, Fldef(d), Fs, Fsb). LFA4 (148–151VC: Fig. 6d and e) gradually transitions from a clearly defined laminated mud with no bioturbation, but frequent >2 mm clasts (Fld), to a bioturbated laminated mud (Flb) to a bioturbated and shell rich stratified mud (Fsb). Flb often consists of wispy, convoluted and/or deformed laminae that contain abundant shell fragments and gravel-sized clasts. Core 148VC contains high angle (>40°) laminae and convoluted bedding with clasts aligning in the coarser silt laminae (Fldef(d): Fig. 6d). A 14C age of $16,860 \pm 221$ cal yrs BP came from a whole bivalve of *Yoldiella* sp. from the Flb facies (151VC: Fig. 6e).

4.2.1.5. LFA5: bioturbated massive mud (Fm, Fmb, Fmg). LFA5 is dark grey (7.5YR 4/1) massive muds (Fm) that are commonly bioturbated (Fmb) and can contain abundant shell fragments (140VC: Fig. 6b). Occasionally beds of gravelly mud (Fmg) interbed with Fs (LFA4). Bioturbation is visually characterised by darker mottles and streaks, but burrows are evident in the X-radiographs. Occasional gravel-sized clasts can be present in this facies, but it is comparatively clast free. Fm is often restricted to a single bed (2–146 cm thick) and is buried by massive shelly sand or gravel (LFA6) with a sharp but convoluted contact. Frequent lenses, pods and burrows filled with the overlying material (LFA6) occur in the upper 10–30 cm of LFA5. LFA5 has a low average shear strength (6 kPa), low wet bulk densities and low magnetic susceptibilities (Fig. 6). Occasionally Fm interbeds with massive, gravelly mud (Fmg) that contains abundant shell fragments and have gradational contacts.

4.2.1.6. LFA6: muddy sand and shelly sand and gravel (Sfm, Sfmb, Sm, Sl, Suf, Gm, Gms). LFA6 is the surface unit across all cores and consists of: massive muddy fine sand (Sfm), bioturbated at times

(Sfmb); massive coarse to fine sand (Sm); laminated sand (Sl); fining-upward sand (Suf); gravel (Gm) and matrix-supported gravel (Gms). The physical properties of these units are typically soft (6 kPa), a low bulk densities and variable magnetic susceptibilities peaking in the gravels (Fig. 6). LFA6 is often rich in shell fragments and variable in thickness.

4.2.2. Lithofacies association (LFA) interpretation

LFA1 is the dominant lithofacies of the outer moraines, GZWs and till sheets that are identified as AFB. They form the broad sediment ridge that spans the outer shelf marking the former extent of the BFIS (Fig. 7). Multiple process interpretations for LFA1 are possible spanning subglacial diamictons over-compacted by grounded ice (Ó Cofaigh et al., 2007, 2013; Evans et al., 2006) to sub-ice shelf diamictons affected by severe iceberg turbation (Domack et al., 1999). IRD rain-out is another possible interpretation, but the over-consolidation of LFA1 indicates that this is not the dominant process. Morphological evidence in the bathymetric data confirm pervasive iceberg scouring of the outer shelf down to water depths of 450 m (Dunlop et al., 2010; Stoker, 1995). The radiocarbon dating sheds some light on the process environment with mixed ages and sequences showing stratigraphic age inversion. The spread of radiocarbon ages between 24.2 ± 0.2 and 12.7 ± 0.1 ka alongside infinite measurements (Fig. 6b), suggest the mixing and compacting of subglacial and ice-marginal diamicton by icebergs. A similar process of iceberg turbation of both subglacial and glaci-marine diamictons occurs in Antarctica and the resultant diamictons are impossible to differentiate (c.f. Powell et al., 1996). Locations protected from iceberg activity, for example by a bounding moraine negate this problem, and the oldest ages in subglacial diamicton from core 125VC (Fig. 6b) provide a maximum constraint on the advance of grounded ice to the shelf edge to after 26.7 ± 0.3 ka BP although this could be as young as 26 ± 0.1 ka BP if using a ΔR of 700 yrs.

The alternating beds of LFA2 (Dmm/Fmd) and LFA3 (Fl) reflect a switch to more clearly discernible glaci-marine sedimentation in an ice-proximal setting. One explanation for this pattern is a seasonal signal capturing the switch in meltwater plume dominated sedimentation during the summer and deposition of ice rafted diamicton from icebergs calving in the winter when meltwater production is lower (Syvitski et al., 1989; Cowan et al., 1997; Cai et al., 1997). An alternative, and favoured, interpretation is that these sediments represent a change from IRD dominated deposition forming sediments of LFA2, to a period of suppressed IRD rainout and meltwater plume dominated sedimentation caused by multiyear sea-ice build-up depositing LFA3 (Ó Cofaigh and Dowdeswell, 2001). Similar interpretations have been made from cores collected in east Greenland (e.g. Jennings and Weiner, 1996; Dowdeswell et al., 2000). The LFA2 beds contain abundant foraminifera for dating and follow a time transgressive pattern with distance from the shelf edge with the oldest deglacial ages from core 146VC, located on the outer shelf, and the youngest from core 149VC located within the Sea of Hebrides. The three ages from core 146VC do not lie in stratigraphic order indicating some downslope remobilisation occurred that is evident in the X-radiographs where a change in clast alignment is visible (Fig. 5). Nevertheless, the dates of 25.9 ± 0.2 and 24.5 ± 0.3 cal ka BP from glaci-marine sediments indicate that this section of the Malin Shelf was free from grounded ice by this time. The oldest age from the inner shelf, 23.2 ± 0.3 ka BP in core 151VC (Fig. 6e), lies directly above AFB and dates the early deglaciation of this part of the Malin Shelf. Finally, a basal age from core 149VC constrains the timing of deglaciation of the Inner Hebrides Trough and indicates that the entire Malin Shelf was free by grounded ice by 20.2 ± 0.2 ka BP.

The muds of LFA4 and LFA5 are interpreted as hemipelagic ice-

distal sediments deposited in an open (glaci)marine environment through the process of suspension settling and occasional IRD contribution. In ice-distal environments, laminated muds often grade into massive bioturbated muds (cf. Jennings, 1993; Svendsen et al., 1992). Only one radiocarbon age dated LFA4 (151VC; Fig. 6e), providing a calibrated age of 16.8 ± 0.2 ka BP indicating that the inner shelf close to Stanton Banks was an ice-distal environment by this time. Lithofacies Fldef in core 148VC, with near vertical laminations, likely represents mass movement of sediment downslope at the core site due to its location in a steep sided bedrock basin.

The sands and gravels of LFA6 are interpreted as postglacial deposits reworked by bottom current activity across the shelf and upper slope (cf. Anderson et al., 1984; Howe et al., 2001). The differing particle size of the matrix and fining upward sequences may represent a weakening of the bottom currents with time (Viana et al., 1998). The shell hash, gravels and massive sands likely represent lag deposits (Dowdeswell et al., 1998). There are no fine glaci-marine sediments preserved on the outer shelf indicating that bottom-current winnowing has been pervasive across the shelf since its deglaciation (Howe et al., 2012).

4.2.3. Lithofacies on the upper continental slope (LFA7–LFA11)

4.2.3.1. LFA7 matrix-supported diamicton (Dmmc). LFA7 forms the basal lithofacies in five cores (118VC, 124VC, 142VC, 143VC, 144VC) and consists of very dark grey (5Y 3/1) sub-rounded to sub-angular gravel to pebble-sized clasts in a very stiff, silty-clay to sandy-silt matrix (Dmmc). Dmmc also contains occasional shell fragments. Core 144VC consists of a 6 m thick Dmmc that has four distinct colour changes with sharp boundaries down core that oscillate from grey to very dark grey from one bed to the next (5Y 4/1 and 5Y 3/1). LFA7 is typically over-consolidated with shear strengths averaging 82 kPa, but can be variable within a core (e.g. 142VC, Fig. 6). LFA7 has also medium wet bulk densities and magnetic susceptibilities (Fig. 6b). LFA7 is dated by nine radiocarbon ages, five of which are finite. The remaining four ages, from core 142VC, are not in stratigraphical order and range between $22,402 \pm 123$ to $18,138 \pm 174$ cal yrs BP (Fig. 6).

4.2.3.2. LFA8: compact stratified, laminated and deformed fine sands and muds (Sl, Ss, Fldef). LFA8 is a dark greyish brown stratified medium to fine silty-sand occurring in two cores (116VC and 124VC). The laminations vary from finely laminated medium sand and silty-sand that form wispy, convoluted lamina to coarser sandier layers that form discontinuous pods and ball and pillow structures (124VC; Fig. 5). Occasional clasts are present towards the base of LFA8. Shear strengths are high, averaging 42 kPa and varying between 13 and 85 kPa. LFA8 has medium wet bulk densities and low magnetic susceptibilities. LFA8 is constrained by three radiocarbon ages, two lying in stratigraphic order from core 116VC ($22,750 \pm 221$ and $18,326 \pm 165$ cal yrs BP) and one from the base of core 124VC ($18,862 \pm 106$ cal yrs BP; Fig. 6a).

4.2.3.3. LFA9: alternating laminated and massive pebbly muds (Fl, Fmd, Fldef). LFA9 only occurs in core 143VC and consists of three lithofacies; finely laminated clay silt with dipping and convoluted laminae (Fldef) as well as planar, horizontal laminations (Fl), which alternates with a massive clast-rich, silty-mud with some grain alignment (Fmd; Fig. 6c). There is no evidence of bioturbation. LFA9 is dark grey (5Y 4/1) and firm with average shear strengths of 23 kPa. A radiocarbon age of $18,090 \pm 174$ cal yrs BP dates the base of the Fl facies.

4.2.3.4. LFA10: bioturbated laminated to massive muds (Flb, Fldef, Fmb). LFA10 consists of three lithofacies; laminated muds that are either bioturbated (Flb) or deformed (Fldef) and massive

bioturbated muds (Fmb). Laminated silts and clays transition from continuous parallel laminae with individual laminae less than 5 mm thick to wispy, discontinuous and more diffuse laminae up-core. Bioturbation is visible as black mottles on the sediment surface that increase in abundance down core and as a dense collection of small irregular burrows to large vertical burrows on the X-radiographs (see Fig. 5). LFA10 is olive grey (5Y 4/2) and has very low shear strengths, wet bulk densities and magnetic susceptibilities. LFA10 also contains low >2 mm clast content (Fig. 6). The oldest age of $22,751 \pm 229$ cal yrs BP dates the Flb facies at the base of core 115VC. A shell age from Fldef in core 116VC produces a younger age of $18,326 \pm 165$ cal yrs BP.

4.2.3.5. LFA11: massive to laminated sands and sandy-gravels (Sl, Sm, Smb, Smg, Gs). LFA11 forms the uppermost lithofacies in seven cores. It is predominantly composed of laminated fine-medium sand (Sl) or massive fine-medium sand (Sm) with gravel to pebble-sized clasts (Smg) and occasional gravel layers (Gs). LFA11 is often bioturbated (Smb), as shown by burrow in the X-radiographs, and contains high concentrations of shell fragments. LFA11 is variable in colour ranging from light olive to dark grey (5Y 4/3, 2.5Y 4/1), has low shear strength, low magnetic susceptibilities and medium wet bulk densities measurements (Fig. 6).

4.2.4. LFA7–LFA11 interpretation

LFA7 is interpreted to be both ice marginal debris flows deposited when the BFIS was at the shelf edge feeding the DBF and postglacial reworking caused by both iceberg turbation and sediment gravity flows. The series of stacked diamicton beds in core 144bVC, and the finite ages collected from this core, are likely examples of stacked ice marginal debris flows (cf. Laberg and Vorren, 1995). Whereas, the variable shear strength measurements combined with the range of ages spanning 22.4 ± 0.1 to 18.1 ± 0.2 ka BP in core 142VC is interpreted as debris flows that were subsequently reworked by icebergs once the BFIS had retreated from the shelf edge.

LFA8 is interpreted as coarse-grained sandy turbidites interbedded with finer-grained muddy turbidites. Although the shear strength in both cores is high we rule out overriding by grounded ice as a cause for this due to the position of the cores on the upper continental slope at ~240 m water depth. Instead, we attribute the high shear strength to compaction during downslope flow and removal of pore water as evident from the water escape structures visible in the X-radiographs (e.g., Fig. 5). We cannot rule out compaction by icebergs but it is likely that icebergs calving from the BFIS would ground on the shallower shelf before reaching the slope.

LFA9 is similar to the alternating LFA2 and LFA3 lithofacies associations except there is only one glaci-marine couplet captured. LFA9 is interpreted to represent a period dominated by suspension settling of turbid water plumes with limited IRD followed by period of IRD delivery combined with suspension settling as described in section 4.3.1. The age of 18.1 ± 0.2 ka BP indicates that IRD was still deposited on the shelf slope at and after this time.

LFA10, characterised by bioturbated laminated muds transitioning to massive bioturbated muds, is interpreted as suspension settling from meltwater plumes. Knutz et al. (2001) noted a similar lithofacies and interpretation in core MD95-2006 taken from the DBF, and dated to after 22 14C ka BP. The basal ages from core 114VC and 116VC correlate with this timing. The lack of sand and coarse sediment and the presence of bioturbation and marine fauna suggest that the grounding line was not marginal at the time of deposition (cf. Ó Cofaigh and Dowdeswell, 2001). The vertical burrows in core 115VC indicate sedimentation was rapid (cf. Jennings et al., 2014). The transition from laminated to massive

bioturbated mud is likely a result of increasing distance from the ice margin and therefore a slowing in the rate of sediment accumulation (Ó Cofaigh and Dowdeswell, 2001).

LFA11 is similar to LFA6 and likely represents postglacial sedimentation. On the slope, cross slope and bottom current reworking are the processes responsible for the deposition of massive and laminated sand, which are a result of both reworking and winnowing of the fine sediments (Faugères and Stow, 1993; Stow et al., 2002).

5. Discussion

5.1. Timing of the maximum BFIS on the Malin Shelf

Our new geophysical data demonstrate that the BFIS reached the shelf edge of over the majority of the Malin Sea. This maximum extent is more widespread than previously figured (Dunlop et al., 2010). A wide and often compound ridge is visible in the bathymetric data (Fig. 7), with GZWs, till sheets and moraines occurring across the shelf edge in the north and south, and near to the shelf edge in the centre of the Malin Shelf. Constraining the timing for this maximum extent has proven challenging with reworked older fauna ubiquitous and iceberg turbation introducing younger specimens to the glacial sediments. On the southern Malin Shelf, the shelf edge moraine provided a protected setting from iceberg turbation, and the youngest radiocarbon dated shell fragments in subglacial diamictos (Core 125VC) constrain shelf edge glaciation to after 26.7 ± 0.3 ka BP. A minimum age is provided by the oldest ages from retreat stage soft diamictos (146VC), thus delimiting shelf edge glaciation to between 26.7 ± 0.3 and 25.9 ± 0.2 ka BP (as late as 25.3 ± 0.3 ka BP if using a ΔR 700 yrs). This timing is very similar to chronologies obtained for shelf edge glaciation elsewhere on the western marine margin of the last British Irish Ice Sheet, with timings of after 26.3 ka BP for the Donegal Ice Stream (Ó Cofaigh et al., submitted), and before 24.3 ka BP in the Celtic Sea (Praeg et al., 2015). A shelf edge position for the BFIS between 26.7 ± 0.3 to 25.9 ± 0.2 ka corresponds with peak IRD flux in core MD95-2006 from the adjacent DBF that also supports a shelf-edge position at ~ 27 ka BP (Knutz et al., 2001; Scourse et al., 2009).

5.2. Iceberg calving history

Radiocarbon dates from iceberg-turbated diamicton on the outer Malin Shelf lie between 24 and 18 ka BP, and point to period of iceberg calving likely associated with the breakup of the BFIS that is equivalent to evidence from other marine-based sectors of the BIIS (Benetti et al., 2010; Dunlop et al., 2010; Ó Cofaigh et al., 2012; Peters et al., 2016). Dunlop et al. (2010) have argued that the lack of iceberg furrows to the east of the Malin Deep suggest that no major calving event took place after the initial breakup of ice on the outer Malin Shelf. Whereas, our chronology for iceberg turbate indicates a period of consistent iceberg activity spanning 6 ka and that the inner Malin Shelf was ice free by 23 ka with iceberg turbation an important process as late as 18 ka. Two of the outer shelf cores (139VC and 125VC) provide a very different chronology for sediments with physical characteristics identical to iceberg-turbated diamicton elsewhere. These sediments (139VC) contain younger samples ranging 15 ± 0.2 to 12.7 ± 0.1 ka BP intermixed with older materials in the range 22.4 ± 0.2 to 24.2 ± 0.2 ka BP (Table 1 and Fig. 6b). Similarly, the youngest age from a reworked shell fragment in these diamictos (125VC) is 12.8 ± 0.1 ka BP. If iceberg turbation was responsible for reworking shell materials into diamictos after 12.7 ± 0.1 ka BP, this supports a view put forward by Small et al. (2013b) for the existence of a marine and calving ice margin in western Scotland during the Younger Dryas Stadial, a cold event

that interrupted the warming and deglaciation of the Northern Hemisphere between 12.9 and 11.7 ka BP (Alley, 2000). If the larger ΔR of 700 yrs is applied to these ages then the youngest age from 139VC would shift from 12662 ± 88 cal yrs BP to 11591 ± 267 cal yrs BP. This is still broadly coeval to the Younger Dryas Stadial and for icebergs reworking the shelf sediments at this time.

To date, understanding of the dynamics and iceberg calving history for the BFIS has relied on IRD records in the DBF (Scourse et al., 2009), which showed: (1) peaks in IRD flux attributed to grounded ice at the shelf edge by 27 ka BP and a maximum mass at 24 ka BP (Scourse et al., 2009); (2) decline in IRD reflecting a rapid ice retreat ~ 23 ka BP; and (3) further peaks in IRD attributed to a shelf wide BFIS readvance between 22 and 16 ka BP. Our retreat history differs showing an early retreat of some 19 km from the shelf edge by 25.9 ka BP, a further ~ 65 km by 23.2 ka BP and with the entire Malin Sea shelf ice free by 20.1 ka BP (Figs. 7 and 8) and even if the larger ΔR of 700 yrs is applied to our chronology, the timing of retreat still occurs earlier (see Table 2) than previously thought. There is no evidence in the acoustic profiles or sediment data for a major readvance back across the shelf between 22 and 16 ka BP. The glacial dynamics associated with IRD flux, e.g. retreat or advance stage, have proven difficult to resolve (Scourse et al., 2009), whereas our sequence of events suggests that greater BFIS-sourced IRD flux to the DBF relates to phases of ice retreat, and as a process, calving dominated the retreat dynamics of the Malin Sea area from 24 to 18 ka BP, with renewed activity during the Younger Dryas Stadial.

5.3. Rates and controls on ice marginal retreat

GZW are associated with temporary pauses in ice-stream retreat or readvances over 10–100 s years and are regarded as representing episodic rather than catastrophic retreat (Dowdeswell and Fugelli, 2012). Two areas of GZW occur on the Malin Shelf, the first at the outer shelf edge and the second at the landward margin of two deep (>170 m) west to east trending troughs landward of the Stanton Banks (Figs. 7 and 5b). Both troughs continue into the Inner Hebrides Trough where water depths increase to >200 m (Fig. 1) and are interpreted as glacial overdeepenings (Dunlop et al., 2010). The GZWs are relatively small, 25 m thick and >10 km wide, but similar-sized GZW occur in other previously glaciated regions e.g., Antarctica (e.g. Anderson and Jakobsson, 2016; Evans and Hogan, 2016; c.f. Table 2 in Batchelor and Dowdeswell, 2015). In those cases their relatively small size is interpreted to reflect either a brief still-stands or a low sediment flux to the grounding zone (Dowdeswell and Fugelli, 2012).

Retreat of ice to the inner of these shelf edge GZWs, GZW1b, occurred after the oldest deglacial age of 25.9 ± 0.2 ka BP (146VC) and a halt in retreat at this GZW likely occurred 25.9 ± 0.2 to 24.8 ± 0.3 ka BP (146VC) based on two mixed benthic foraminifera ages taken from IRD-rich sediments overlying consolidated diamictos. Landward of the overdeepenings and inshore of the Stanton Banks topographical high (Fig. 4b) a series of GZWs step back in a southeast direction and glacial marine sediments in front of these marginal positions have basal ages ranging 23.2 ± 0.3 to 22.1 ± 0.3 ka BP indicating ice-free conditions by this time on the inner shelf. There are no obvious moraines or GZWs visible in the available regional bathymetry (Fig. 7), which reflects rapid retreat of the BFIS across these deeper waters and their reverse slopes. Previous research has pointed to early and rapid deglaciation of the inner Malin Shelf (Binns et al., 1974), but the radiocarbon dating targeted bulk carbon and the ages were dismissed as too old (Harkness and Wilson, 1979). Later attempts to constrain ice-free conditions in other marine cores from the southern Inner Hebrides and western Scotland were significantly younger (Peacock,

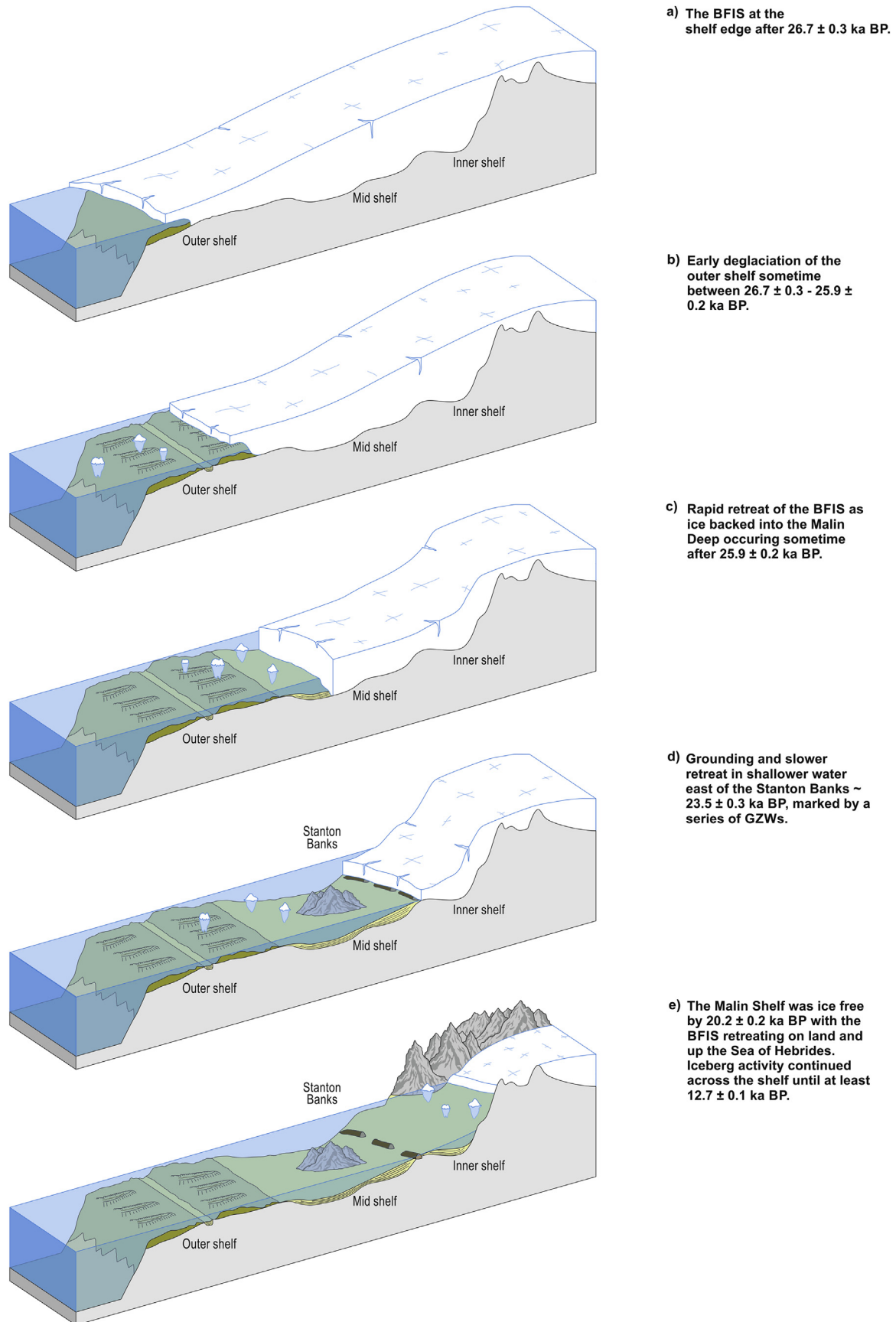


Fig. 8. Schematic diagram of the retreating BFIS from (a) its last glacial maximum extent position at 26.7 ± 0.3 ka BP, (b) early deglaciation and second grounding line position on the outer shelf between 26.7 ± 0.3 – 25.9 ± 0.2 ka BP, (c) rapid retreat back through the deep troughs, (d) mid-shelf grounding position at 23.5 ± 0.3 ka BP and (e) retreat onto the coastline by 20 ka BP.

2008; Peacock et al., 2012). Our eastern most deglacial age (149VC; Fig. 6a) confirms this early deglaciation of the inner shelf by 20.2 ± 0.2 ka BP. This timing is supported by terrestrial evidence that deglaciation was already underway by 20.6 ka on Tíree ~20 km to the east (Small et al., 2017). ^{36}Cl exposure ages from southern Skye show complete deglaciation by 17.6 ka (Small et al., 2016) and so a fully deglaciated Malin Shelf by 20.2 ± 0.2 ka BP fits the existing regional onshore geochronology. Radiocarbon and cosmogenic nuclide dates from onshore the north coast of Ireland suggest that ice stepped back on land by at least ~20 ka in this region (McCabe and Clark, 2003; Clark et al., 2009).

5.4. Forcing and conditioning of the retreat dynamics of the BFIS

The deglaciation of the Malin Shelf coincides with a period of global sea-level lowering (Lambeck et al., 2014) and local cooling of sea-surface temperature (Peck et al., 2008; Hibbert et al., 2010). A prevailing hypothesis for the 'early' deglaciation of the BIIS is the influence of Heinrich Event 2 (H2), which is associated with a 15–30 m global sea-level rise caused by the collapse of the Laurentide Ice Sheet (Chappell, 2002; Siddall et al., 2003). This sea-level rise would have destabilised the marine-based portions of the BIIS calving front (Scourse et al., 2009). Furthermore, Mg/Ca sea-surface temperature estimates and percent of *Neogloboquadrina pachyderma* sinistral coiling (NPS %), a proxy for the polar front, show a northward migration of the polar front at the same time (Peck et al., 2008). This migration of the polar front allowed warmer waters to reach the calving margin of the BIIS during Greenland Stadial 2 (GS2) at 23 ka BP (Scourse et al., 2009). However, our data indicate that the BFIS had already retreated from its shelf-edge position and was located ~100 km further inland at the time of H2. Therefore, H2 and the migration of the polar front cannot explain the timing of initial retreat from the shelf edge, although both likely had an influence on the continued retreat of the BFIS.

An alternative mechanism for early retreat is an increase in relative sea level (RSL) caused by local isostatic loading and crustal deformation of the Malin Shelf by the BFIS. Subsequently, this RSL rise would have led to the destabilisation and retreat of the ice margin (cf. Eyles and McCabe, 1989). The majority of the Malin Shelf was ice free by 20.2 ± 0.2 ka BP (at latest 19.4 ± 0.2 ka BP if using a ΔR 700 yrs), and our shallowest core (153VC) is ~20 m above the global sea level minima of 134 m between 29 and 21 ka BP (Lambeck et al., 2014). Given this core has glacial marine material dated at 22.6 ± 0.3 ka BP it indicates that the glacial isostatic loading of this portion of the Malin Shelf was at least 20 m and likely significantly more for the laminated glacial marine muds to be deposited without wave based erosion or iceberg turbation of the sediments. This suggests relative sea level was at least ~15 m higher than is currently modelled for this region at 21 ka BP (Bradley et al., 2011). Thus, although global sea levels at the LGM were ~134 m lower than present (Lambeck et al., 2014), the outer Malin Shelf (120–150 m and 160 m at the shelf break) would have still been below sea level. The effect of glacial isostatic adjustment (GIA) on the outer shelf between 27 and 21 ka BP has not been modelled with any degree of certainty, but existing models extending back to 21 ka BP suggest that the outer shelf was still responding to ice loading at this time (Bradley et al., 2011). Theoretical treatments and modelled simulations show that the stability of marine-based ice sheets is closely coupled with the depth of water at the grounding line (Schoof, 2007). A reduction in sea level can be enough to stop retreat, and an increase in sea level can cause instability and enhance retreat (Gomez et al., 2012). We argue that the RSL rise associated with this isostatic loading would be significant enough to cause the destabilisation of the BFIS, a

conclusion consistent with those put forward by Eyles and McCabe (1989).

Topographical controls leave a clear signature in the retreat history of the BFIS, with episodic retreat and minor re-advances on the topographical highs of the outer shelf. Furthermore, we hypothesise that the more rapid and continued retreat across the mid shelf was aided by the presence of the two east-to-west trending troughs, the Malin Deep south of the Stanton Banks and the second trough to the north that connects to the Inner Hebrides Trough. These over-deepened troughs were likely formed by ice streaming over several glacial periods (Davies et al., 1984; Dunlop et al., 2010) across the softer bedrock (Permian to Cretaceous strata) cropping out in that sector. Much more resistant Dalradian basement bedrock crops out on the outer shelf (Fyfe et al., 1993) and likely contributed in the formation a reverse slope, with greater erosion of the softer lithologies (c.f. Cook and Swift, 2012). This geometry of the ice-stream bed is likely to focus and enhance calving of the ice margin as it retreated back into deeper waters, thus providing a mechanism for rapid and irreversible retreat (c.f. Jamieson et al., 2012). The ice-bed topography of the Malin Shelf was, therefore, a significant factor in the early demise and pace of ice marginal retreat of the BFIS.

6. Conclusion

- By directly dating glacial landforms and sediments on the shelf, the data presented here provides the best constraint on the extent and timing of retreat of the last BFIS, a major draining system of the BIIS across the Malin Shelf.
- Glacial geomorphic features evident on the sub-bottom profiles confirm that the BFIS reached the shelf edge during the last glacial period and its maximum extent sometime before 25.9 ± 0.2 ka BP
- Retreat across the shelf is marked by a series of large GZWs and smaller moraines and at least one still-stand that occurred sometime $\sim 25.9 \pm 0.2$ – 24.8 ± 0.3 ka BP. The outer and mid Malin Shelf was free of grounded ice by 23.2 ± 0.3 ka BP, with the inner shelf ice free by 20.2 ± 0.2 ka BP.
- We conclude that the initial retreat of BFIS was caused by the growth of the BIIS that increased isostatic loading on the Malin Sea shelf leading to a relative sea-level rise. Additionally, topographic control in the form of over-deepened basins likely facilitated enhanced calving of the BFIS leading to rapid and irreversible retreat of this ice stream once it started to retreat into deeper water. It is likely that the impact of H2 and the northward migration of the Polar front at 23 ka BP aided further retreat of the BFIS; however they cannot be the cause of its initial demise.

Acknowledgments

This research was funded by the UK Natural Environment Research Council grant; BRITICE-CHRONO NE/J009768/1. The work was supported by the NERC Radiocarbon Facility (allocation numbers 1722.0613 and 1878.1014). Thanks are due to the staff at the NERC AMS Laboratory, East Kilbride for carbon isotope measurements. We thank the officers and crew of the RRS *James Cook* for their help with acquisition and the British Geological Survey for vibrocore collection during the cruise JC106. We also thank Kasper Weilbach, Riccardo Arosio, Catriona Purcell, Zoe Roseby and Elke Hanenkamp for their scientific support on the JC106 leg 2 cruise and to Chris Orton (Design and Imaging Unit at Durham University) who drafted Fig. 8. The two anonymous reviewers are thanks for their detailed and constructive comments.

Appendix A. Supplementary data

Supplementary data to this article can be found online at <https://doi.org/10.1016/j.quascirev.2018.10.002>.

References

- Alley, R.B., 2000. The Younger Dryas cold interval as viewed from central Greenland. *Quat. Sci. Rev.* 19, 213–226.
- Anderson, J.B., Brake, C.F., Myers, N.C., 1984. Sedimentation on the Ross Sea continental shelf, Antarctica. *Mar. Geol.* 57, 295–333.
- Anderson, J.B., Jakobsson, M., 2016. Grounding-zone Wedges on Antarctic Continental Shelves, vol. 46. Geological Society, London, Memoirs, pp. 243–244.
- Austin, W.E.N., Bard, E., Hunt, J.B., Kroon, D., Peacock, J.D., 1995. The ^{14}C age of the Icelandic Vedde Ash: implications for Younger Dryas marine reservoir age corrections. *Radiocarbon* 37, 53–62.
- Batchelor, C.L., Dowdeswell, J.A., Hogan, K.A., 2011. Late Quaternary ice flow and sediment delivery through Hinlopen Trough, Northern Svalbard margin: submarine landforms and depositional fan. *Mar. Geol.* 284, 13–27.
- Batchelor, C.L., Dowdeswell, J.A., 2015. Ice-sheet grounding-zone wedges (GZWs) on high-latitude continental margins. *Mar. Geol.* 363, 65–92.
- Benetti, S., Dunlop, P., Ó Cofaigh, C., 2010. Glacial and glacially-related features on the continental margin of northwest Ireland mapped from marine geophysical data. *J. Maps* 6 (1), 14–29.
- Binns, P.E., Harland, R., Hughes, M.J., 1974. Glacial and post-glacial sedimentation in the sea of Hebrides. *Nature* 48, 751–754.
- Bradwell, T., Stoker, M.S., Colledge, N.R., Wilson, C.K., Merritt, J.W., Long, D., Everest, J.D., Hestvik, O.B., Stevenson, A.G., Hubbard, A.L., Finlayson, A.G., Mathers, H.E., 2008. The northern sector of the last British Ice Sheet: maximum extent and demise. *Earth Sci. Rev.* 88, 207–226.
- Bradley, S.L., Milne, G.A., Shennan, I., Edwards, R., 2011. An improved glacial isostatic adjustment model for the British Isles. *J. Quat. Sci.* 26, 541–552.
- Brooks, A.J., Bradley, S.L., Edwards, R.J., Milne, G.A., Horton, B., Shennan, I., 2008. Postglacial relative sea-level observations from Ireland and their role in glacial rebound modelling. *J. Quat. Sci.* 23, 175–192.
- Cai, J., Powell, R.D., Cowan, E.A., Carlson, P., 1997. Lithofacies and seismic-reflection interpretation of temperate glacial marine sedimentation in Tarr Inlet, Glacier Bay, Alaska. *Mar. Geol.* 143, 5–37.
- Chappell, J., 2002. Sea level changes forced ice breakouts in the Last Glacial cycle: new results from coral terraces. *Quat. Sci. Rev.* 21, 1229–1240.
- Clark, P.U., Dyke, A.S., Shakun, J.D., Carlson, A.E., Clark, J., Wohlfarth, B., Mitrovica, J.X., Hostetler, S.W., McCabe, A.M., 2009. The last glacial maximum. *Science* 325 (5941), 710–714.
- Clark, C.D., Hughes, A.L., Greenwood, S.L., Jordan, C., Sejrup, H.P., 2012. Pattern and timing of retreat of the last British-Irish ice sheet. *Quat. Sci. Rev.* 44, 112–146.
- Clark, C.D., Ely, J.C., Greenwood, S.L., Hughes, A.L.C., Meehan, R., Barr, I.D., Bateman, M.D., Bradwell, T., Doole, J., Evans, D.J.A., Jordan, C.J., Monteys, X., Pellicer, X.M., Sheehy, M., 2017. BRITICE Glacial Map, Version 2: a Map and GIS Database of Glacial Landforms of the Last British–Irish Ice Sheet. <https://doi.org/10.1111/bor.12273>. ISSN 0300-9483.
- Cook, S.J., Swift, D.A., 2012. Subglacial basins: their origin and importance in glacial systems and landscapes. *Earth Sci. Rev.* 115, 332–372.
- Cowan, E.A., Cai, J., Powell, R.D., Clark, J.D., Pitcher, J.N., 1997. Temperate glacial marine varves: an example from Disenchantment Bay, southern Alaska. *J. Sediment. Res.* 67, 536–549.
- Davies, H.C., Dobson, M.R., Whittington, R.J., 1984. A revised seismic stratigraphy for Quaternary deposits on the inner continental shelf west of Scotland between 55°30'N and 57°30'N. *Boreas* 13, 49–66.
- Dobson, M.R., Whittington, R.J., 1992. Aspects of the Geology of the Malin Sea Area, vol. 62. Geological Society Special Publication, pp. 291–311.
- Domack, E.W., Jacobson, E.A., Shipp, S., Anderson, J.B., 1999. Late pleistocene–Holocene retreat of the west Antarctic ice-sheet system in the Ross sea: Part 2—sedimentologic and stratigraphic signature. *Geol. Soc. Am. Bull.* 111, 1517–1536.
- Dooley, H.D., Crease, J., 1978. Observed and Geostrophic Currents South and East of Faroe during Overflow '73, p. 53. ICES CM 1978/C.
- Dove, D., Arosio, R., Finlayson, A., Bradwell, T., Howe, J.A., 2015. Submarine glacial landforms record late pleistocene ice-sheet dynamics, inner Hebrides, Scotland. *Quat. Sci. Rev.* 123, 76–90.
- Dowdeswell, J., Fugelli, E., 2012. The seismic architecture and geometry of grounding-zone wedges formed at the marine margins of past ice sheets. *Geol. Soc. Am. Bull.* 124, 1750–1761.
- Dowdeswell, J.A., Elverhøi, A., Spjelhagen, R., 1998. Glacial marine sedimentary processes and facies on the polar North Atlantic margins. *Quat. Sci. Rev.* 17, 243–272.
- Dowdeswell, J.A., Whittington, R.J., Jennings, A.E., Andrews, J.T., Mackensen, A., Marienfeld, P., 2000. An origin for laminated glacial marine sediments through sea-ice build-up and suppressed iceberg rafting. *Sedimentology* 47, 557–576.
- Dowdeswell, J.A., Evans, J., Ó Cofaigh, C., 2010. Submarine landforms and shallow acoustic stratigraphy of a 400 km-long fjord-shelf-slope transect, Kangerlussuaq margin, East Greenland. *Quat. Sci. Rev.* 29, 3359–3369.
- Dunlop, P., Shannon, R., McCabe, M., Quinn, R., Doyle, E., 2010. Marine geophysical evidence for ice sheet extension and recession on the Malin Shelf: new evidence for the western limits of the British Irish ice sheet. *Mar. Geol.* 276, 86–99.
- Ellett, D.J., 1979. Some oceanographic features of Hebridean waters. *Proceedings of the Royal Society of Edinburgh* 77B, 61–74.
- Elverhøi, A., Norem, H., Andersen, E.S., Dowdeswell, J.A., Fossen, I., Hafliðason, H., Kenyon, N.H., Laberg, J.S., King, E.L., Sejrup, H.P., Solheim, A., Vorren, T., 1997. On the origin and flow behaviour of submarine slides on deep-sea fans on the Norwegian–Barents Sea continental margin. *Geo Mar. Lett.* 17, 119–125.
- Evans, D.J.A., Phillips, E.R., Hiemstra, J.F., Auton, C.A., 2006. Subglacial till: formation, sedimentary characteristics and classification. *Earth Sci. Rev.* 78, 115–176.
- Evans, J., Hogan, K.A., 2016. Grounding-zone Wedges on the Northern Larsen Shelf, Antarctic Peninsula, vol. 46. Geological Society, London, Memoirs, pp. 237–238.
- Eyles, N., Eyles, C.H., Miall, A.D., 1983. Lithofacies types and vertical profile models; an alternative approach to the description and environmental interpretation of glacial diamict and diamictite sequences. *Sedimentology* 30, 393–410.
- Eyles, N., McCabe, A.M., 1989. The Late Devensian (< 22,000 BP) Irish Sea Basin: the sedimentary record of a collapsed ice sheet margin. *Quat. Sci. Rev.* 8, 307–351.
- Faugères, J.-C., Stow, D.A., 1993. Bottom-current-controlled sedimentation: a synthesis on the contourite problem. *Sediment. Geol.* 82, 287–297.
- Finlayson, A., Fabel, D., Bradwell, T., Sugden, D., 2014. Growth and decay of a marine terminating sector of the last British-Irish Ice Sheet: a geomorphological reconstruction. *Quat. Sci. Rev.* 83, 28–45.
- Fyfe, J.A., Long, D., Evans, D., 1993. The Geology of the Malin-Hebrides Sea Area. HMSO for the British Geological Survey, London.
- Gomez, N., Pollard, D., Mitrovica, J.X., Huybers, P., Clark, P.U., 2012. Evolution of a coupled marine ice sheet–sea level model. *J. Geophys. Res.* 117, F01013.
- Harkness, D.D., Wilson, H.W., 1979. Scottish universities research and reactor centre radiocarbon measurements III. *Radiocarbon* 21, 203–256.
- Hedges, R.E.M., Housley, R.A., Law, I.A., Perry, C., Hendy, E., 1988. Radiocarbon dates from the oxford AMS system: archaeometry datelist 9. *Archaeometry* 30, 291–305.
- Hibbert, F.D., Austin, W.E.N., Leng, M.J., Gatloff, R.W., 2010. British ice sheet dynamics inferred from north Atlantic ice-rafted debris records spanning the last 175,000 years. *J. Quat. Sci.* 25, 461–482.
- Hindmarsh, R.C.A., 2018. Ice sheets and glacier modelling. In: Menzies, J., van der Meer, J.J.M. (Eds.), *Past Glacial Environments*. Elsevier Ltd., Amsterdam, pp. 605–661.
- Hogan, K.A., Dowdeswell, J., Ó Cofaigh, C., 2012. Glacial marine sedimentary processes and depositional environments in an embayment fed by West Greenland ice streams. *Mar. Geol.* 311, 1–16.
- Hogan, K.A., Ó Cofaigh, C., Jennings, A.E., Dowdeswell, J.A., Hiemstra, J.F., 2016. Deglaciation of a major palaeo-ice stream in disko trough, west Greenland. *Quat. Sci. Rev.* 147, 5–26.
- Howe, J.A., Dove, D., Bradwell, T., Gafeira, J., 2012. Submarine geomorphology and glacial history of the Sea of the Hebrides, UK. *Mar. Geol.* 315, 64–76.
- Howe, J.A., Stoker, M.S., Woolfe, K.J., 2001. Deep-marine seabed erosion and gravel lags in the northwestern Rockall trough, North Atlantic ocean. *J. Geol. Soc.* 158, 427.
- Huthnance, J.M., 1986. Rockall slope current and shelf edge processes. *Proc. R. Soc. Edinburgh* 88B, 83–101.
- Jamieson, S.S.R., Viela, A., Livingstone, S.J., Ó Cofaigh, C., Stokes, C., Hillenbrand, C.-D., Dowdeswell, J.A., 2012. Ice-stream stability on a reverse bed slope. *Nat. Geosci.* 5, 799–802.
- Jennings, A.E., 1993. The quaternary history of Cumberland sound, southeastern Baffin island: the marine evidence. *GeHographie Physique et Quaternaire* 47, 21–42.
- Jennings, A.E., Weiner, N.J., 1996. Environmental change in eastern Greenland during the last 1300 years: evidence from foraminifera and lithofacies in Nansen Fjord 683N. *Holocene* 6, 179–191.
- Jennings, A.E., Walton, M.E., Ó Cofaigh, C., Kilfeather, A., Andrews, J.T., Ortiz, J.D., De Vernal, A., Dowdeswell, J.A., 2014. Palaeoenvironments during younger dryas-early Holocene retreat of Greenland ice sheet from outer Disko trough, central west Greenland. *J. Quat. Sci.* 29, 27–40.
- Joughin, I., Smith, B.E., Medley, B., 2014. Marine ice sheet collapse potentially under way for the Thwaites Glacier Basin, West Antarctica. *Science* 344, 735–738.
- Knutz, P.C., Austin, W.E., Jones, E.J.W., 2001. Millennial-scale depositional cycles related to British ice sheet variability and north Atlantic paleocirculation since 45 kyr BP, Barra fan, UK margin. *Paleoceanography* 16, 53–64.
- Kroon, D., Simmiel, G., Austin, W.E.N., Derrick, S., Knutz, P., Simmiel, T., 2000. Century- to millennial-scale sedimentological–geochemical records of glacial–Holocene sediment variations from the Barra Fan (NE Atlantic). *J. Geol. Soc.* 157, 643–653.
- Laberg, J.S., Vorren, T.O., 1995. Late Weichselian submarine debris flow deposits on the bear island trough mouth fan. *Mar. Geol.* 127, 45–72.
- Lambeck, K., Rouby, H., Purcell, A., Sun, Y., Sambridge, M., 2014. Sea level and global ice volumes from the last glacial maximum to the Holocene. *Proc. Natl. Acad. Sci. U. S. A.* 111, 15296e15303.
- McCabe, A.M., Clark, P.U., 2003. Deglacial chronology from County Donegal, Ireland: implications for deglaciation of the British–Irish ice sheet. *J. Geol. Soc.* 160, 847–855.
- Mouginot, J., Rignot, E., Scheuchl, B., Fenty, I., Khazendar, A., Morlighem, M., Buzzi, A., Paden, J., 2015. Fast retreat of Zachariæ Isstrøm, northeast Greenland. *Science* 350, 1357–1361.
- Ó Cofaigh, C., Dowdeswell, J.A., 2001. Laminated sediments in glacial marine environments: diagnostic criteria for their interpretation. *Quat. Sci. Rev.* 20,

- 1411–1436.
- Ó Cofaigh, C., Evans, J., Dowdeswell, J.A., Larter, R.D., 2007. Till characteristics, genesis and transport beneath Antarctic paleo-ice streams. *J. Geophys. Res.* 112.
- Ó Cofaigh, C., Dunlop, P., Benetti, S., 2012. Marine geophysical evidence for Late Pleistocene ice sheet extent and recession off northwest Ireland. *Quat. Sci. Rev.* 44, 147–159.
- Ó Cofaigh, C., Andrews, J., Jennings, A., Dowdeswell, J., Hogan, K., Kilfeather, A., Sheldon, C., 2013. Glacimarine lithofacies, provenance and depositional processes on a West Greenland trough-mouth fan. *Journal of Quaternary Science* 28, 13–26.
- Ó Cofaigh, C., Hogan, K.A., Dowdeswell, J.A., Streuff, K., 2016. Stratified Glacimarine Basin-fills in West Greenland Fjords, vol. 46. Geological Society, London, Memoirs, pp. 99–100.
- Peacock, J.D., 2008. Late Devensian palaeoenvironmental changes in the sea area adjacent to Islay, SW Scotland: implications for the deglacial history of the island. *Scott. J. Geol.* 44, 183–190.
- Peacock, J.D., Austin, W.E.N., Selby, I., Graham, D.K., Harland, R., Wilkinson, I.P., 1992. Late Devensian and flandrian palaeoenvironmental changes on the Scottish continental shelf west of the outer Hebrides. *J. Quat. Sci.* 7, 145–161.
- Peacock, J.D., Horne, D.J., Whittaker, J.E., 2012. Late Devensian evolution of the marine offshore environment of western Scotland. *Proc. Geologists' Assoc.* 123, 419–437.
- Peck, V.L., Hall, I.R., Zahn, R., Elderfield, H., Grousset, F., Hemming, S.R., Scourse, J.D., 2006. High resolution evidence for linkages between NW European ice sheet instability and Atlantic meridional overturning circulation. *Earth Planet Sci. Lett.* 243, 476–488.
- Peck, V.L., Hall, I.R., Zahn, R., Elderfield, H., 2008. Millennial-scale surface and subsurface paleothermometry from the northeast Atlantic, 55e8 ka BP. *Paleoceanography* 23, PA3221.
- Peters, J.L., Benetti, S., Dunlop, P., Ó Cofaigh, C., 2015. Maximum extent and dynamic behaviour of the last British Irish ice sheet west of Ireland. *Quat. Sci. Rev.* 128, 48–68.
- Peters, J.L., Benetti, S., Dunlop, P., Ó Cofaigh, C., Moreton, S.G., Wheeler, A.J., Clark, C.D., 2016. Sedimentology and chronology of the advance and retreat of the last British-Irish Ice Sheet on the continental shelf west of Ireland. *Quat. Sci. Rev.* 140, 101–124.
- Powell, R.D., Dawber, M., McInnes, J.N., Pyne, A.R., 1996. Observations of the grounding-line area at a floating glacier terminus. *Ann. Glaciol.* 22, 217–223.
- Praeg, D., McCarron, S., Dove, D., Ó Cofaigh, C., Scott, G., Monteys, X., Facchin, L., Romeo, R., Coxon, 2015. Ice sheet extension to the Celtic Sea shelf edge at the last glacial maximum. *Quat. Sci. Rev.* 111, 107–112.
- Reid, D.G., Turrell, W.R., Walsh, M., Corten, A., 1997. Cross-shelf processes north of Scotland in relation to the southerly migration of Western mackerel. *ICES (Int. Counc. Explor. Sea) J. Mar. Sci.* 54, 168–178.
- Reimer, P.J., Bard, E., Bayliss, A., Beck, J.W., Blackwell, P.G., Ramsey, C.B., Buck, H., Cheng, H., Edwards, R.L., Friedrich, M., Grootes, P.M., Guilderson, T.P., Hafildason, H., Hajdas, I., Hatté, C., Heaton, T.J., Hoffman, D.L., Hogg, A.G., Hughen, K.A., Kaiser, K.F., Kromer, B., McCormac, F.G., Manning, S.W., Nui, M., Reimer, R.W., Richards, D.A., Scott, E.M., Southon, J.R., Staff, R.A., Turney, C.S.M., van der Plicht, J., 2013. Intcal13 and Marine13 radiocarbon age calibration curves, 0–50,000 years Cal Bp. *Radiocarbon* 55, 1869–1887.
- Sacchetti, F., Benetti, S., Georgiopoulou, A., Shannon, P.M., O'Reilly, B.M., Dunlop, P., Quinn, R., Ó Cofaigh, C., 2012. Deep-water geomorphology of the glaciated Irish margin from high-resolution marine geophysical data. *Mar. Geol.* 291–294, 113–131.
- Schoof, C., 2007. Ice sheet grounding line dynamics: steady states, stability, and hysteresis. *J. Geophys. Res.* 112, F03S28. <https://doi.org/10.1029/2006JF000664>.
- Scourse, J.D., Haapaniemi, A.I., Colmenero-Hidalgo, E., Peck, V.L., Hall, I.R., Austin, W.E., Knutz, P.C., Zahn, R., 2009. Growth, dynamics and deglaciation of the last British–Irish ice sheet: the deep-sea ice-rafted detritus record. *Quat. Sci. Rev.* 28, 3066–3084.
- Selby, I., 1989. Quaternary Geology of the Hebridian Continental Margin. Unpublished PhD thesis. Nottingham University.
- Siddall, M., Rohling, E.J., Almogi-Labin, A., Hemleben, C., Meischner, D., Schmelzer, I., Smeed, D.A., 2003. Sea-level fluctuations of the last glacial cycle. *Nature* 423, 853–858.
- Singarayer, J.S., Richards, D.A., Ridgwell, A., Valdes, P.J., Austin, W.E.N., Beck, J.W., 2008. An oceanic origin for the increase of atmospheric radiocarbon during the Younger Dryas. *Geophys. Res. Lett.* 35, L14707.
- Small, D., Austin, W., Rinterknecht, V., 2013a. Freshwater influx, hydrographic reorganization and the dispersal of ice-rafted detritus in the sub-polar North Atlantic Ocean during the last deglaciation. *J. Quat. Sci.* 28, 527–535.
- Small, D., Parrish, R.R., Austin, W.E.N.A., Cawood, P.A., Rinterknecht, V., 2013b. Provenance of North Atlantic ice rafted debris during the last deglaciation - a new application of U-Pb rutile and zircon geochronology. *Geology* 41, 155–158.
- Small, D., Rinterknecht, V., Austin, W.E.N., Bates, C.R., Benn, D.I., Scourse, J.D., Bourlès, D.L., ASTER Team, Hibbert, F.D., 2016. Implications of ³⁶Cl exposure ages from Skye, northwest Scotland for the timing of ice stream deglaciation and deglacial ice dynamics. *Quat. Sci. Rev.* 150, 130–145.
- Small, D., Benetti, S., Dove, D., Ballantyne, C.K., Fabel, D., Clark, C.D., Gheorghiu, D.M., Newall, J., Xu, S., 2017. Cosmogenic exposure age constraints on deglaciation and flow behaviour of a marine-based ice stream in western Scotland, 21–16 ka. *Quat. Sci. Rev.* 167, 30–46.
- Stoker, M.S., 1995. The influence of glacial sedimentation on slope-apron development on the continental margin off NW Britain. In: Scrutton, R.A., Stoker, M.S., Shimmield, G.B., Tudhope, A.W. (Eds.), *The Tectonics, Sedimentation and Palaeoceanography of the North Atlantic Region*, vol. 90. Geological Society London, pp. 159–177. Special Publication.
- Stoker, M.S., Hitchen, K., Graham, C.C., 1993. United Kingdom Offshore Regional Report: the Geology of the Hebrides and West Shetland Shelves and Adjacent Deep-water Areas. HMSO for the British Geological Survey, London.
- Stow, D.A.V., Faugères, J.-C., Howe, J.A., Pudsey, C.J., Viana, A., 2002. Bottom currents, contourites and deep sea sediment drifts: current state-of-the-art. *Geological Society of London Memoirs* 22, 7–20.
- Svendsen, J.I., Mangerud, J., Elverhøim, A., Solheim, A., Schiøllhelm, R.T.E., 1992. The Late Weichselian glacial maximum on western Spitsbergen inferred from offshore sediment cores. *Mar. Geol.* 104, 1–17.
- Syvitski, J.P.M., Farrow, G.E., Atkinson, R.J.A., Moore, P.G., Andrews, J.T., 1989. Baffin Island fjord macrobenthos: bottom communities and environmental significance. *Arctic* 42, 232–247.
- Viana, A.R., Faugères, J.-C., Stow, D.A.V., 1998. Bottom-current-controlled sand deposits - a review of modern shallow-to deep-water environments. *Sediment. Geol.* 115, 53–80.
- Wanamaker Jr., A.D., Butler, P.G., Scourse, J.D., Heinemeier, J., Eiríksson, J., Knudsen, K.L., Richardson, C.A., 2012. Surface changes in the North Atlantic meridional overturning circulation during the last millennium. *Nat. Commun.* 3, 899.
- Wilson, L.J., Austin, W.E.N., Jansen, E., 2002. The last British Ice Sheet: growth, maximum extent and deglaciation. *Polar Res.* 21, 243–250.
- Winkelmann, D., Schäfer, C., Stein, R., Mackensen, A., 2008. Terrigenous events and climate history of the Sophia basin, Arctic ocean. *G-cubed* 9, Q07023.